COHERENT IMAGE FORMATION APPLIED TO THE DESIGN OF FOURIER TRANSFORM ELEMENTS

by

Bernard Steven Fritz

A Thesis Submitted to the Faculty of the

COMMITTEE ON OPTICAL SCIENCES (GRADUATE)

In Partial Fulfillment of the Requirements
For the Degree of

MASTER OF SCIENCE

In the Graduate College

THE UNIVERSITY OF ARIZONA

1 9 8 0

STATEMENT BY AUTHOR

This thesis has been submitted in partial fulfillment of requirements for an advanced degree at The University of Arizona and is deposited in the University Library to be made available to borrowers under rules of the Library.

Brief quotations from this thesis are allowable without special permission, provided that accurate acknowledgment of source is made. Requests for permission for extended quotation from or reproduction of this manuscript in whole or in part may be granted by the head of the major department or the Dean of the Graduate College when in his judgment the proposed use of the material is in the interests of scholarship. In all other instances, however, permission must be obtained from the author.

SIGNED: Bernard L. Evans

APPROVAL BY THESIS DIRECTOR

This thesis has been approved on the date shown below:

Roland V. Shack — 4/14/80

ROLAND V. SHACK
Professor of Optical Sciences

Date

ACKNOWLEDGMENTS

I wish to express appreciation to the faculty and staff of the Optical Sciences Center, especially my advisor Dr. Roland V. Shack.

I am deeply indebted to my wife, Teresa, who put up with me during this undertaking and provided the encouragement to finish. Discussions with Bill Chen and Kevin Thompson were quite helpful.

TABLE OF CONTENTS

TABLE OF CONTENTS, Continued.

LIST OF ILLUSTRATIONS

LIST OF ILLUSTRATIONS, Continued.

LIST OF TABLES

ABSTRACT

Coherent image formation is discussed and how it applies to the design of Fourier transform lenses. Relationship between the pupil aberrations and image aberrations was used to simplify design considerations. Several designs are included to demonstrate the concepts. In the initial lens layout 1st order tools of the Y-$\overline{Y}$ diagram and Vander Lugt notation were used. The primary goal in the designs was to reduce the object-Fourier transform distance without losing the Fourier transform quality.

CHAPTER 1

INTRODUCTION

The concept of optical filtering was introduced by the works of Abbe and Lord Rayleigh around the turn of the century. Both noticed a curious behavior associated with the image in the experimental setup pictured in Fig. 1.1.

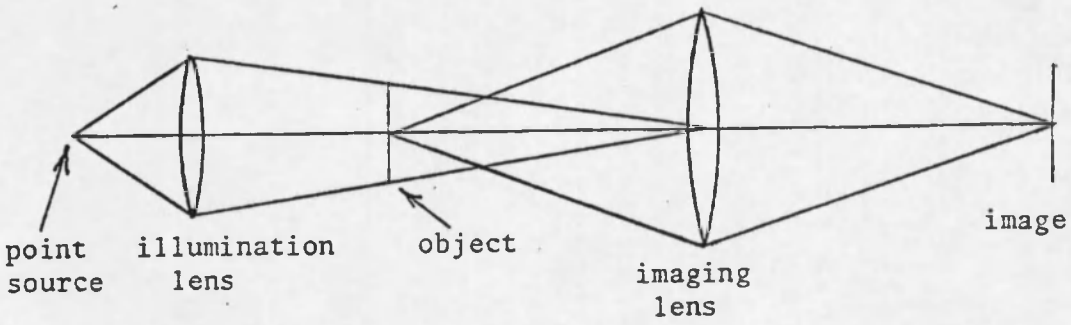

Fig. 1.1. Köhler illumination.

It was found that larger aperture imaging lenses resulted in images of higher resolution than smaller aperture imaging lenses even though the cone of light emanating from the light source filled only a very small central portion of the aperture, leaving the remaining outer portion of the aperture apparently unused. Abbe discovered that the influence of the aperture resulted from diffraction caused by the object detail whose dimensions were comparable to the wavelength of light, causing the angles of diffraction to become so large that light

actually filled the dark space of the aperture. Recognizing this, Abbe developed his theory of image formation. According to Abbe's theory only a certain portion of the diffraction components generated by a highly structured object are intercepted by the finite entrance pupil, and only these components contribute to the final image. With these ideas in hand Abbe designed a series of large aperture lenses with aberration correction for axial points. The imagery for these lenses was worse than he expected. This led Abbe to the study of imaging surface elements perpendicular to the axis and he found sharp imagery occurred only under specific conditions. For conjugate points, the ratio of the sines of the two angles must be constant for all zones of the aperture. This came to be known as the Abbe sine condition. With the fulfillment of this additional requirement Abbe found the lens achieved the desired performance.

Abbe's theory of image formation was dealt with in terms of Fourier methods in the work of Duffieux (1946) in France and later by O'Neill (1956) in the United States. They dealt with coherent imagery only in the paraxial approximation, and showed the Fourier transform properties of ideal lenses. This laid the foundation for the Fourier optics treatment of coherent imaging systems (Goodman, 1968). The inherent ability of a lens to produce a two-dimensional Fourier transform (F.T.) was a remarkable property and was put to use in applications such as synthetic-aperture radar. Coherent optical systems, in particular F. T. elements, are limited to the paraxial approximation in a Fourier optics treatment. Design beyond the paraxial approximation

has generally been described only with respect to how the system performance deteriorates as the paraxial approximation breaks down (Vatz, 1977). The F. T. properties of a lens beyond the paraxial domain were presented by Blandford (1970), who recognized a need for the correction of two sets of conjugates of the lens. This work was then followed by other publications dealing with the same idea.

The purpose of this thesis is to put forth certain basic design approaches for coherent optical systems, such as the F. T. lens, if one is interested in performance beyond the paraxial approximation.

The idea for this work came from a study of the procedure for reducing the object-F. T. distance in a F. T. lens while maintaining all other system parameters including the F. T. quality. During this time a discussion with R. V. Shack, Optical Sciences Center, University of Arizona, on the conjugate shift equations was found to be very useful in understanding the design considerations for F. T. elements. At this same time the work of Hopkins (1976) on a non-Gaussian type of image theory was found to generalize the F. T. element design greatly. Both of these investigations were used in formulating a scheme by which general F. T. elements should be designed. These topics are dealt with in Chapter 2 along with various examples to show the validity of these concepts. Tools for 1st order design of coherent optical systems are presented in Chapter 3 with primary emphasis on F. T. elements. Actual design examples of F. T. elements are given in Chapters 4 and 5 with the main objective that of reducing the object-F. T. distance while maintaining the desired image quality.

CHAPTER 2

COHERENT IMAGE FORMATION

A linear systems description of image formation requires that the optical system be linear and shift invariant. In the case of incoherent illumination both these conditions are satisfied if the system is isoplanatic (free from field dependent aberrations) and the image formation is considered in terms of intensity. For coherent illumination the linearity condition is met if one deals with complex amplitude. The shift invariance condition is, however, not as easily met.

In order to define clearly the meaning of the phase difference between points of a diffraction image one must specify a surface of reference. In most previous descriptions the reference surfaces were the Gaussian object and image planes. Thus a Gaussian theory of image formation was being developed by means of linear system theory. It was found in this case that if the system was isoplanatic and also the illuminating point source was imaged into the pupil of the system (matched illumination) that this system was indeed shift-invariant in complex amplitude, if one observed the image on a surface confocal with the exit pupil. See Fig. 2.1. These ideas are all covered in a recent book by Gaskill (1978). In this approach a F. T. relationship between the object plane's transmittance and the entrance pupil sphere is described, and in image space between the exit pupil sphere and the

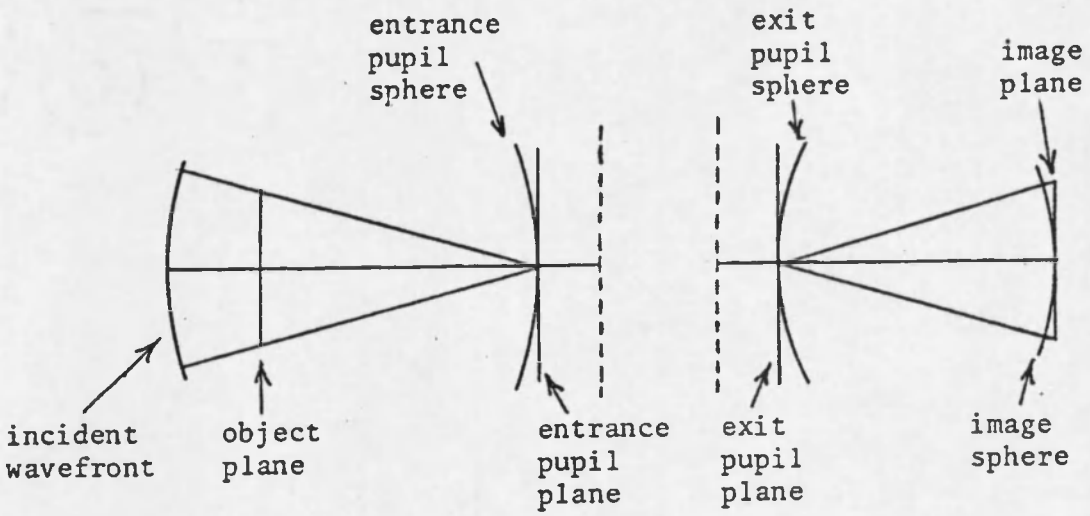

Fig. 2.1. Gaussian ideal.

image sphere. Remember, though, that this approach to image formation is based on the Gaussian ideal (collinear transformation). It is in fact not truly shift-invariant in complex amplitude for extra-paraxial regions. The chosen references surfaces were inappropriate for a proper representation of diffraction theory of image formation.

The proper reference surfaces are confocal to the entrance and exit pupils. This system is now truly shift-invariant in complex amplitude. See Fig. 2.2. The Sine ideal (Hopkins, 1976) applies to this kind of image formation. In the Sine ideal representation the angular variables in the paraxial ray trace equations are the sines of finite angles. The Sine ideal eliminates the piston (phase) error associated with off-axis points which prevented the previous development in the Gaussian ideal from being shift-invariant. The two developments become

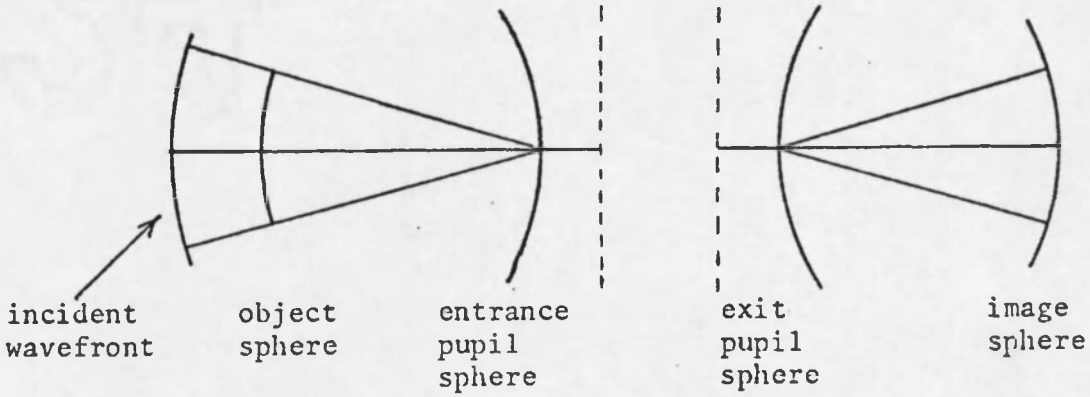

Fig. 2.2. Sine ideal.

equivalent if the object is at infinity and the system is telecentric in image space. This type of system will play a major role in F. T. lens design. If one is only interested in a 1st order approximation to shift-invariance then the isoplantic condition reduces to the absence of linear coma. The object and image spheres reduce to planes, and again the two developments are equivalent. For the Sine ideal a F. T. relationship exists between the complex amplitude of the object sphere and entrance pupil sphere (Hopkins, 1977). One thus sees that a F. T. of the object always exists in a coherent imaging system due to the process of diffraction. Thus in the design of a F. T. lens the goal is to image the entrance pupil sphere onto the exit pupil sphere with the minimal amount of aberration. One must be careful now in the discussion of aberrations to avoid confusion in dealing with the two imaging theories, the Sine ideal and the Gaussian ideal.

Linear System Approach

Linear system theory may be used to obtain a relationship between the impulse response of the image sphere and the impulse response of the exit pupil sphere. The basic configuration is shown in Fig. 2.3. If perfect matched illumination is present, one may relate the object sphere and entrance pupil sphere disturbances, and also the exit pupil sphere disturbances, by a F. T. dependence. This gives the entrance pupil $\Phi_1(R_1)$ and exit pupil $\Phi_2(R_2)$ disturbances as

$$\Phi_1(R_1) = \int_{-\infty}^{\infty} \phi_1(r_1)\, e^{-iR_1 \cdot r_1}\, dr_1 = \mathcal{F}\{\phi_1(r_1)\}$$

$$\Phi_2(R_2) = \int_{-\infty}^{\infty} \phi_2(r_2)\, e^{-iR_2 \cdot r_2}\, dr_2 = \mathcal{F}\{\phi_2(r_2)\} \quad .$$

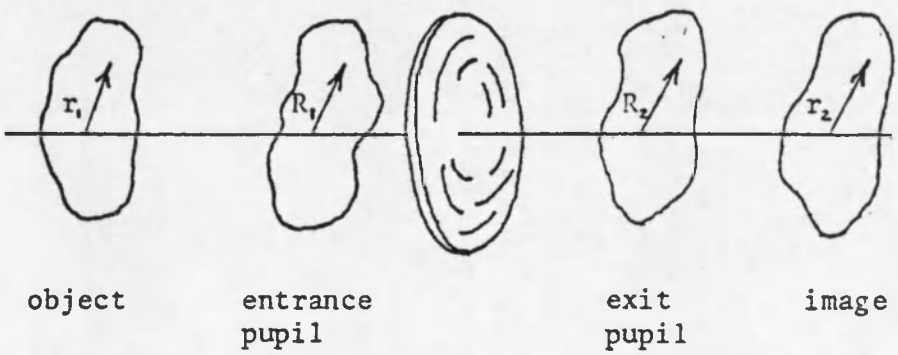

Fig. 2.3. General optical system.

Let the impulse response for the object sphere imagery be $g_{21}(r_2;r_1)$ and $G_{21}(R_2;R_1)$ for the pupil sphere imagery.

$$\phi_2(r_2) = \int_{-\infty}^{\infty} g_{21}(r_2;r_1)\phi_1(r_1)\, dr_1$$

$$\Phi_2(R_2) = \int_{-\infty}^{\infty} G_{21}(R_2;R_1)\Phi_1(R_1)\, dR_1 \ .$$

Using the inverse F. T. relationship one finds that

$$\phi_1(r_1) = \frac{1}{4\pi^2} \int_{\infty}^{\infty} \Phi_1(R_1)\, e^{iR_1\circ r_1}\, dR_1 \ .$$

Substituting this into the expression for $\phi_2(r_2)$

$$\phi_2(r_2) = \int_{-\infty}^{\infty} g_{21}(r_2;r_1) \left[\frac{1}{4\pi^2} \int \Phi_1(R_1)\, e^{iR_1\circ r_1}\, dR_1\right] dr_1$$

$$\phi_2(r_2) = \frac{1}{4\pi^2} \iint_{-\infty}^{\infty} g_{21}(r_2;r_1)\ \Phi_1(R_1)\ e^{iR_1\circ r_1}\, dR_1 dr_1$$

and taking the F. T. of this expression we find

$$\Phi_2(R_2) = \frac{1}{4\pi^2} \iiint_{-\infty}^{\infty} g_{21}(r_2;r_1)\ \Phi_1(R_1)\ e^{iR_1\circ r_1}\ e^{-iR_2\circ r_2} dR_1 dr_1 dr_2$$

$$\int_{-\infty}^{\infty} G_{21}(R_2;R_1)\ \Phi(R_1)\, dR_1 = \frac{1}{4\pi^2} \iiint_{-\infty}^{\infty} g_{21}(r_2;r_1)\ \Phi(R_1)\ e^{-i(R_2\circ r_2 - R_1\circ r_1)}\, dR_1 dr_1 dr_2$$

which reduces to

$$G_{21}(R_2;R_1) = \frac{1}{4\pi^2} \iint_{-\infty}^{\infty} g_{21}(r_2;r_1)\ e^{-i(R_2\circ r_2 - R_1\circ r_1)}\ dr_1 dr_2 \ .$$

A similar equation can be found for $g_{21}(r_2;r_1)$

$$g_{21}(r_2;r_1) = \frac{1}{4\pi^2} \iint_{-\infty}^{\infty} G_{21}(R_2;R_1)\, e^{i(R_2\circ r_2 - R_1\circ r_1)}\, dR_1 dR_2 \circ$$

These equations relate the impulse responses of the image and pupils. If one assumes that $g_{21}(r_2;r_1)$ is shift-invariant

$$h_{21}(r_2-r_1) = g_{21}(r_2;r_1)$$

then

$$\phi_2(r_2) = \int_{-\infty}^{\infty} h_{21}(r_2-r_1)\,\phi_1(r_1)\,dr_1$$

$$\Phi_2(R_2) = H_{21}(R_2)\,\Phi_2(R_2)$$

$$\Phi_2(R_2) = \int_{-\infty}^{\infty} G_{21}(R_2;R_1)\,\Phi_1(R_1)\,dR_1 \circ$$

Thus

$$G_{21}(R_2;R_1) = H_{21}(R_2)\,\delta(R_2-R_1) \circ$$

If the image is diffraction limited $H_{21}(R_2) = \mathrm{CYL}\,(DR_2)$

then $G_{21}(R_2;R_1) = \delta(R_2-R_1)\ \mathrm{CYL}(DR_2) \circ$

This result asserts that if stigmatic imagery exists for the image sphere then the pupil imagery will have no phase errors and also be stigmatic. Thus a relationship between the object and pupil imagery does exist. We will first look at this relationship in terms of the Gaussian ideal since this is more familiar. Wynne (1952) and more recently Welford (1974) dealt with this relationship in discussing conjugate shift equations and pupil aberrations. The pupil aberrations

are used in the development of the conjugate shift equations, which are presented in Appendix A.

S_{VI} Piston Error

In Wynne's work the pupil spherical aberration $\bar{S}_I$ has been equated with S_{VI} piston error of the image. It appears that a contribution to S_{VI} from Petzval curvature has been neglected, as pointed out by Shack (1979). Wynne gives

$$S_{VI} = \bar{S}_I$$

while Shack gives

$$S_{VI} = \bar{S}_I - \left(\frac{\bar{A}}{A}\right)\text{Ж}\Delta(\bar{u}^2) - \left(\frac{\bar{A}}{A}\right)^2\text{Ж}^2\text{P} \quad .$$

First one must decide exactly what S_{VI} represents in the Gaussian ideal representation. Mathematically S_{VI} corresponds to the last of the six terms in the 4th order wave aberration expansion. Since S_{VI} has no pupil dependence it does not appear in the ray aberration contributions. Physically S_{VI} represents a phase error between different points of the field, or the OPD between the chief ray and the axial ray of the system. In order for the S_{VI} aberration to have proper meaning one must deal with the object sphere as a reference surface, whereas the other aberrations of the group deal with a plane object surface. Thus it appears S_{VI} only has meaning in the Sine ideal viewpoint or when the object is at infinity. The following example will be used to point out the problem.

Consider a single refracting surface with the stop at the center of curvature and the object a finite distance away (see Fig. 2.4).

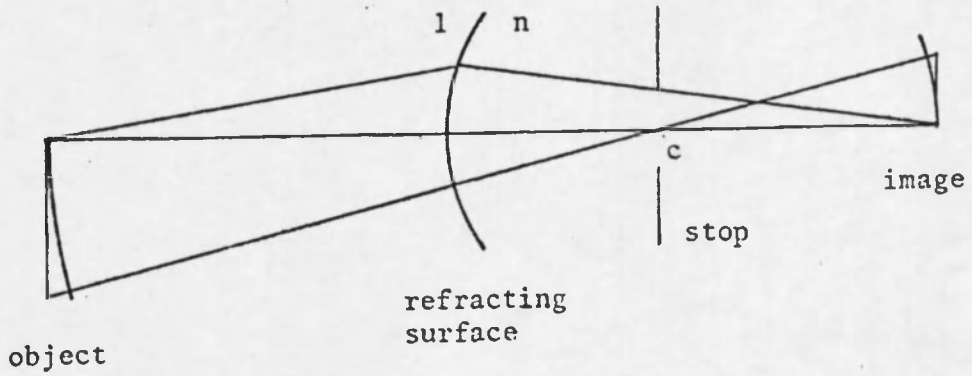

Fig. 2.4. Piston error case I.

Both Shack and Welford give $S_{VI} = 0$ in this case for a plane object, but this is obviously not the case. If one deals instead with the object sphere and image sphere, then clearly $S_{VI} = 0$. In order to point out the difference between Shack's and Wynne's S_{VI} term one must be consistent such that all the 4th order wave aberrations remain valid. If the object moves to infinity the object sphere will degenerate to a plane, thus making things consistent (see Fig. 2.5).

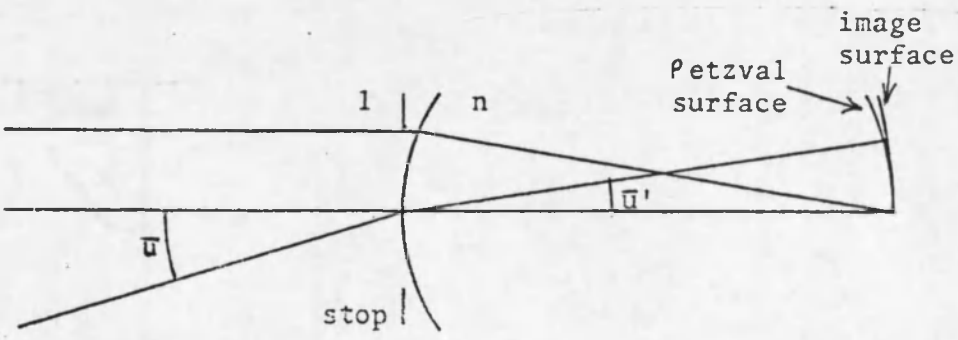

Fig. 2.5. Piston error case II.

Now the stop is shifted to the refracting surface (see Fig. 2.6). Shack's value for S_{VI} is non-zero due to the contribution to piston error by the Petzval curvature. In this case Shack gives

$$S_{VI} = \frac{-n^2\bar{u}'^4}{c} - \frac{n^3\bar{u}'^4}{c} + \frac{2n^4\bar{u}'^4}{c}$$

To check this the system was set up on ACCOSV and run with the following parameters:

$$c = .04 \qquad n = 1.5 \qquad \bar{u} = 3°$$

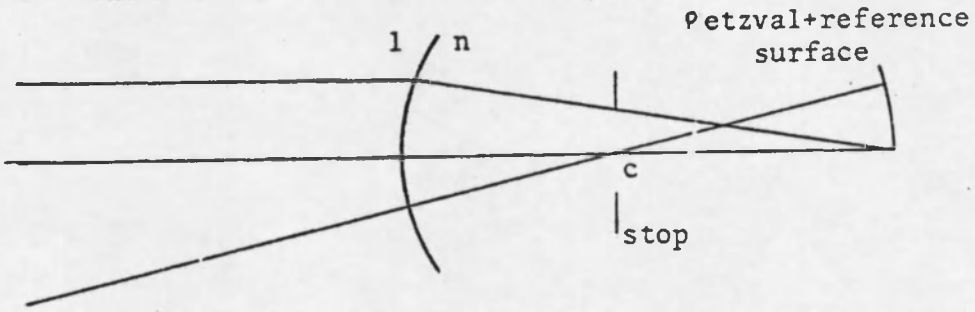

Fig. 2.6. Piston error case III.

Wynne $\bar{S}_I = 0, \quad S_{VI} = 0$

Shack $\bar{S}_I = 0, \quad S_{VI} \neq 0$

A real ray was traced on axis to the image point and a real chief ray was traced to the Petzval surface. The OPD between these two rays is the phase error, and will be represented to 4th order by the wave aberration coefficients W_{200} and W_{400}. W_{200} is the sag between the Petzval surface and the image sphere.

$$OPD = 112.5mm - 112.465754mm = .034246mm$$

$$W_{200} = n^2 r\, u^2/2 = .03426446mm$$

$$S_{VI} = \frac{\bar{u}'^4}{c}(2n^4 - n^3 - n^2)$$

$$W_{400} = \frac{S_{VI}}{8} = -.000020878$$

$$W_{400} + W_{200} = .0342485mm$$

We find very good agreement between the calculated and ray trace values of S_{VI}.

Pupil Aberrations

Now that we know how to apply the Gaussian ideal properly to coherent optical systems, let's return to the assertion that if stigmatic imagery exists between the object sphere and image sphere then stigmatic imagery exists between the pupil spheres, and examine it to 4th order. The connecting relations (Appendix A) are

SPHERICAL $$S_I = \bar{S}_{VI} - \left(\frac{A}{\bar{A}}\right) \mathcal{H}\, \Delta(u^2) - \left(\frac{A}{\bar{A}}\right)^2 S_{IV}$$

COMA $$S_{II} = \bar{S}_V - \mathcal{H}\, \Delta(u^2)$$

ASTIGMATISM $$S_{III} = \bar{S}_{III} - \mathcal{H}\, \Delta(u\bar{u})$$

PETZVAL $$S_{IV} = \bar{S}_{IV}$$

DISTORTION $$S_V = \bar{S}_{II} - \mathcal{H}\, \Delta(\bar{u}^2)$$

PISTON $$S_{VI} = \bar{S}_I - \left(\frac{\bar{A}}{A}\right) \mathcal{H}\, \Delta(\bar{u}^2) + \left(\frac{\bar{A}}{A}\right)^2 S_{IV}$$

At first appearance these relations seem to contradict the assertion, but one must remember that Seidel's equations are based on the Gaussian ideal, or plane to plane imagery. This is where the contradiction lies and can be explained if the pupil sphere and image sphere can be made planes, as in the case of a system with the object at infinity and telecentric in image space. This system is pictured in Fig. 2.7.

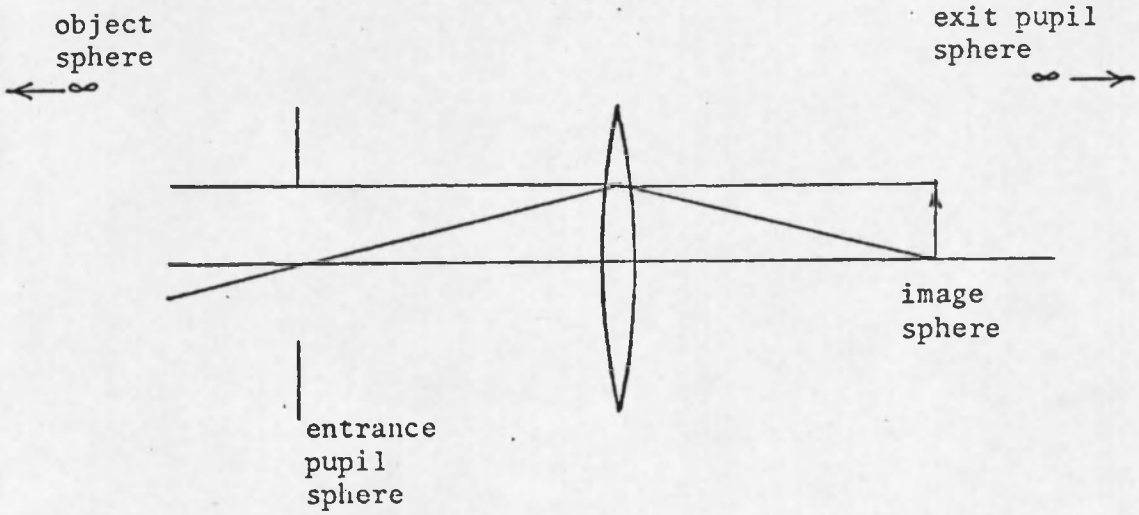

Fig. 2.7. Telecentric system.

One is to show that for this system

$$\text{If } S_I = 0 \qquad \text{Then } \overline{S}_I = 0$$
$$S_{II} = 0 \qquad \overline{S}_{II} = 0$$
$$S_{III} = 0 \qquad \overline{S}_{III} = 0$$
$$S_{IV} = 0 \qquad \overline{S}_{IV} = 0$$
$$S_V = K \qquad \overline{S}_V = K$$
$$S_{VI} = 0 \qquad \overline{S}_{VI} = 0$$

Notice that S_V and $\overline{S}_V$ have non-zero values. The reason for this is that the Sine ideal follows a sine law dependence whereas Gaussian imagery follows a tangent law. If the Petzval surface is confocal to the exit pupil then $S_{VI} = \overline{S}_I$. Thus $S_I = 0$ requires $\overline{S}_{VI} = 0$ and $S_{VI} = 0$ requires $\overline{S}_I = 0$. The Petzval terms both will be zero ($S_{IV} = \overline{S}_{IV} = 0$). We see that $\bar{u}' = 0$ and $u = 0$, which makes the quantity $\Delta(u\bar{u})$ zero and thus if $S_{III} = 0$ then $\overline{S}_{III} = 0$. If $S_{II} = 0$ then $\overline{S}_V = \mathcal{H}\Delta(u^2)$. Knowing that the sine law is to hold, $S_V = \mathcal{H}\Delta(\bar{u}^2)$ requires $\overline{S}_{II} = 0$.

A triplet lens was designed using the above ideas. In the design distortion was given the proper target value $S_V = \mathcal{H}\Delta(u^2)$ and S_{VI} was controlled by making the OPL of the chief ray equal to that of an axial ray, both originating from the entrance pupil and terminating at the Petzval surface. The other Seidel coefficients were given target values of zero. The thin lens design was obtained as shown in Table 2.1. Good agreement with theory was found upon turning the lens around and looking at pupil imagery. The aberrations were

$$\overline{W}_{040} = -2.6\ \lambda$$

$$\overline{W}_{131} = .0016\ \lambda$$

$$\overline{W}_{222} = -.0069\ \lambda$$

$$\overline{W}_{311} = -3.1\ \lambda$$

$$\overline{W}_{220} = -.068\ \lambda$$

$$W_{400} = \overline{W}_{040} = \frac{1}{8}\overline{S}_I = \frac{1}{8}\frac{\overline{SA3}}{F/\#} = -2.6\ \lambda$$

Table 2.1. Telecentric asymmetrical triplet design.

EFL	BFD	FFD	F/#	Field
600 mm	492.9 mm	142.3 mm	10	2.9°

Surface	Curvature	Distance	Index
1	.003316		1.788
2	.000641		
3	-.002367	160.6	1.517
4	.005998		
5	.001079	187.8	1.788
6	.002761		

λ = .58756 μm

W_{040} = -.029 λ

W_{131} = .38 λ

W_{222} = -.14 λ

W_{311} = 2.9 λ

W_{220} = -.068 λ

W_{400} = -2.6 λ

Another system showing this characteristic is the Offner system (1975). This is an afocal double-telecentric system and is pictured in Fig. 2.8. The system is made up of two mirrors concentric about c with one mirror having half the radius of the other. For the image all of the Seidel aberrations excepting the phase error S_{VI} are zero and for the pupil sphere only $\overline{S}_I$ and $\overline{S}_V$ are nonzero. The finite value of $\overline{S}_V$ is due to the Sine ideal. The S_{VI} and $\overline{S}_I$ can both be corrected by adding an aspheric corrector plate at the object plane.

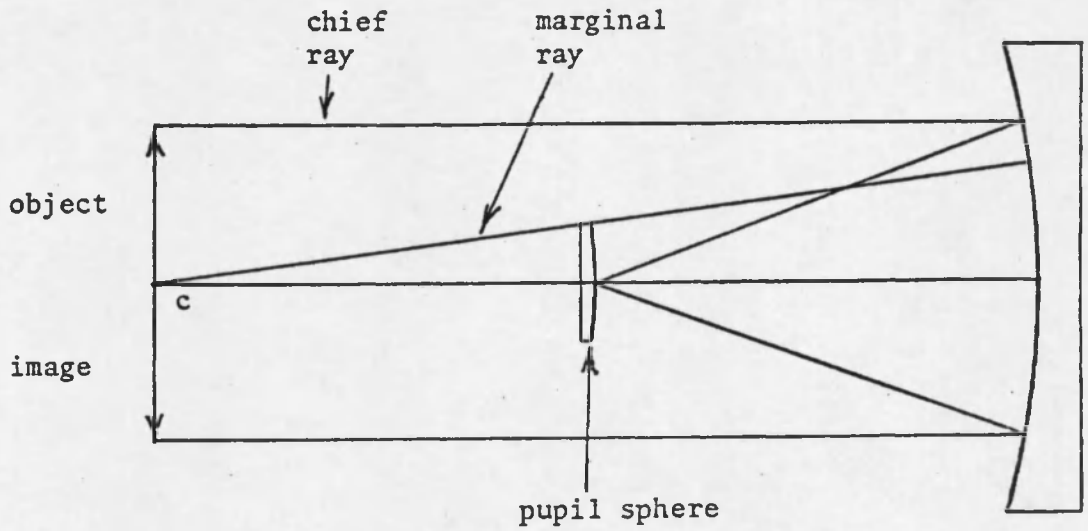

Fig. 2.8. Optical layout of the Offner system.

F. T. Elements

Let's take the ideas developed up to this point and apply them to the design of F. T. lenses. A Sine ideal optical system is pictured in Fig. 2.9. The objects F.T. exists on the entrance pupil sphere and is imaged to the exit pupil sphere by the optical system. If there is to be no phase error present on the exit pupil sphere (ignoring Petzval curvature), S_I must be zero. If the mapping from entrance to exit pupil sphere is to be distortion free then

$$\frac{h'}{h} = \frac{\ell_4 \sin U'}{\ell_1 \sin U} = \text{constant} = \frac{\ell_4 u'}{\ell_1 u}$$

which gives

$$\frac{\sin U'}{u'} = \frac{\sin U}{u}$$

Abbe sine condition

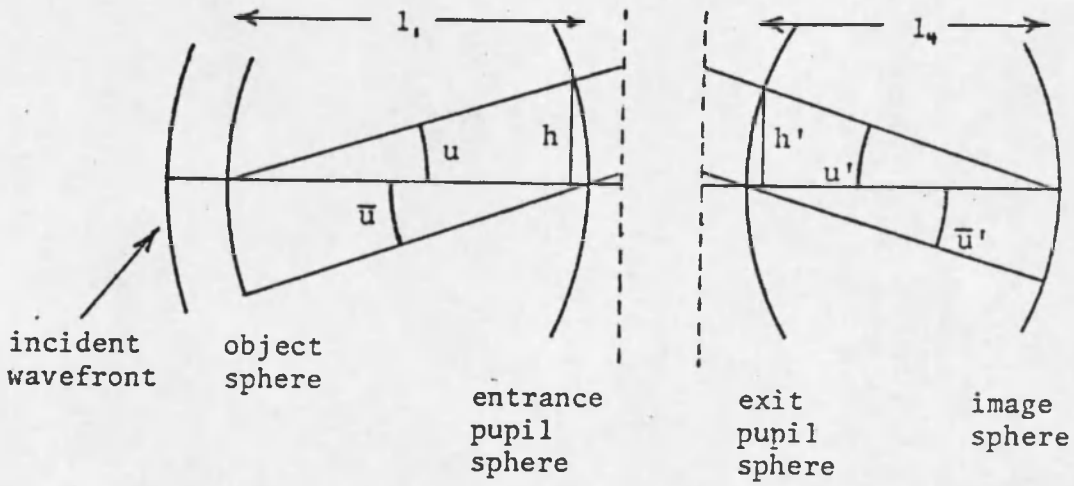

Fig. 2.9. 1st order parameters of a Sine ideal system.

Thus we see the relationship between S_{II} and $\bar{S}_V$. For $S_{II} = 0$ the finite value of $\bar{S}_V$ is due to the fact that distortion is zero on the pupil sphere, not the pupil plane. This can be seen in the following derivation using Fig. 2.10. If no distortion exists on the exit pupil sphere the value present on the exit pupil plane will be

sag of exit pupil sphere $\quad \Delta z = \dfrac{h'^2}{2\ell'}$ $\qquad \dfrac{h'}{\ell'} = u'$ PARAXIAL

$$D = u'\Delta z = \frac{h'}{\ell'}\,\Delta z$$

$$= \frac{h'^3}{2\ell'^2} = \frac{h'u'}{2} \qquad \text{Ж} = h'\bar{u}'n'$$

optical path difference

$$\bar{W}_{311} = \Delta(n\bar{u}D) = -\Delta\left(\frac{n'\bar{u}'h'u'^2}{2}\right) = \frac{n'\bar{u}'h'}{2}\,\Delta(u^2)$$

$$\bar{W}_{311} = \frac{\text{Ж}}{2}\,\Delta(u^2)$$

$$\bar{S}_V = \text{Ж}\,\Delta(u^2)$$

the same value given by the equation $S_{II} = \bar{S}_V - \text{Ж}\Delta(u^2)$ for $S_{II} = 0$.

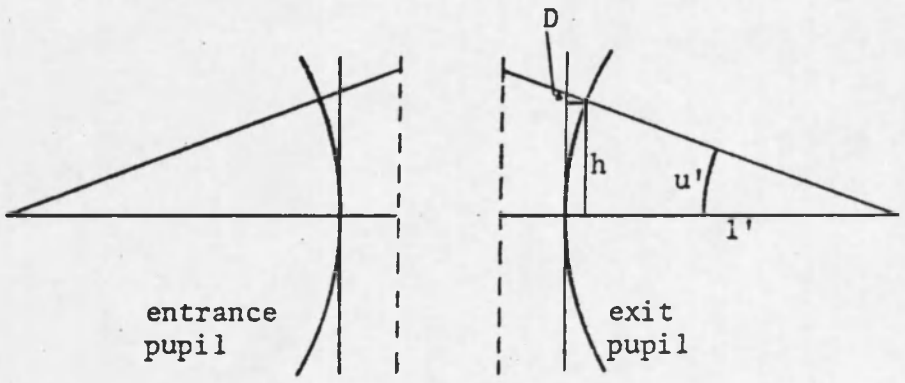

Fig. 2.10. Pupil plane distortion.

If one is to design in terms of a Gaussian ideal, the F.T. lens is going to have a finite value of distortion associated with it. This value is given by $\overline{S}_V = \mathcal{H}\Delta(u^2)$ and implies zero coma (S_{II}) in the image plane. In designing a F.T. lens one is correcting both the image and pupil conjugates. It was shown in a previous section that if one of these conjugate sets has perfect correction then the other will also be perfectly corrected. In theory then one would correct one set for all aberrations including phase error and the design would be finished. In actual designs however one balances aberrations against each other and rarely can obtain perfect correction for one set of conjugates, thus not allowing one to take advantage of the above fact. This means both conjugates must be corrected separately. However, the design can be simplified if the system is made symmetrical with respect to these conjugates such that the imagery for one set is identical to the other. This means if the image magnification is m the pupil magnification is

1/m and the lens elements are symmetrical. The most practical F.T. system is one in which the phase curvature associated with the F.T. system is zero. This is the common "f-f" system where a plane object located 1 focal length away from the lens is illuminated with collimated light and the F.T. of the object exists in the rear focal plane. This system is shown in Fig. 2.11.

In this type of system the object and pupil spheres have become planes, so Gaussian based aberration theory, and thus normal lens design programs, may be used in the design. If, however, one is interested in a more general type of system, non-planar illumination, then a Sine ideal approach must be used in the design. For coherent image formation the Sine ideal must be used in all cases except that shown in Fig. 2.12, which is the only Gaussian ideal system which can be shift-invariant in complex amplitude.

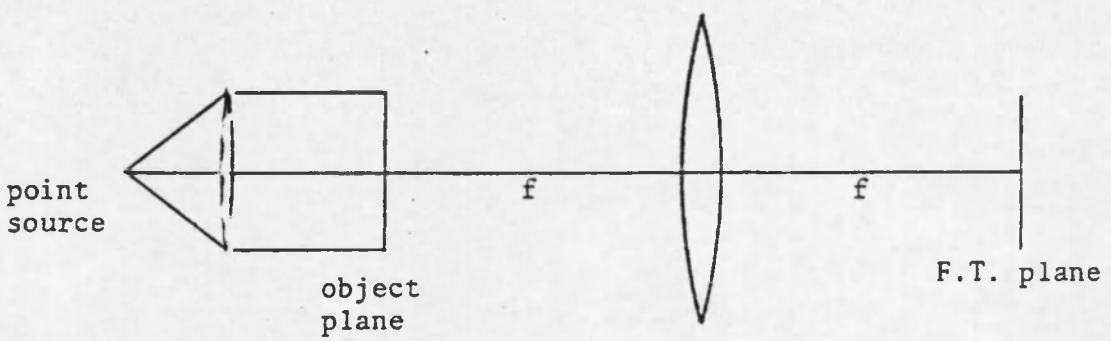

Fig. 2.11. "f-f" system.

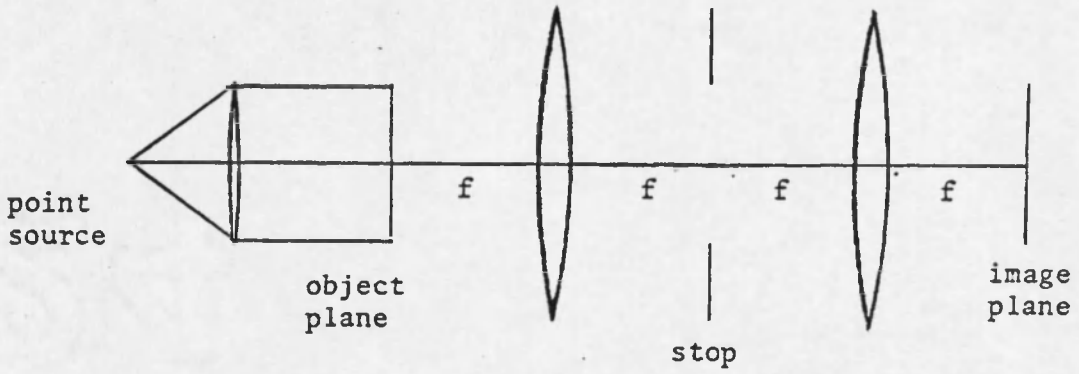

Fig. 2.12. Shift-invariant Gaussian ideal.

CHAPTER 3

1ST ORDER LAYOUT

Introduction

Two useful tools are available for the 1st order layout of F.T. lenses and coherent imaging systems. The first of these is the Y-$\bar{Y}$ diagram developed by Delano (1963), which is a graphic method of representing the 1st order properties of any optical system of axially symmetric refracting or reflecting surfaces. The second is the operational notation developed by Vander Lugt (1966), which characterizes basic optical elements as block diagrams and is a linear systems treatment of image formation. These methods complement each other in the synthesizing and analysis of optical systems, with the Y-$\bar{Y}$ diagram representing the geometrical optical nature of the system and the Vander Lugt notation of the physical optical nature.

Y-$\bar{Y}$ Diagram

The Y-$\bar{Y}$ diagram consists of a two-dimensional cartesian plot of the paraxial marginal ray heights (y) versus the paraxial chief ray heights ($\bar{y}$) of an optical system. A simple system and its Y-$\bar{Y}$ diagram is shown in Fig. 3.1. This Y-$\bar{Y}$ diagram is made up of two line segments, the first representing the object space and the second the image space, which intersect at the optical element location.

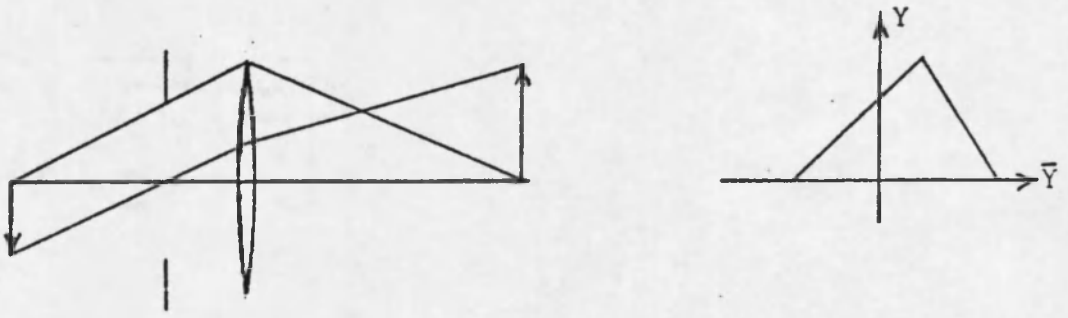

Fig. 3.1. Single element system and its Y-$\bar{Y}$ diagram.

Wherever one of these line segments crosses the $\bar{y}$-axis, an object or image is located, and where the y-axis is crossed a stop or pupil is located. The separation of any two points along the line segments correspond to axial separation in the actual layout. Twice the area of the triangle formed by these points and the origin is equal to $\mathcal{H}\tau$, the product of the Lagrange invariant $\mathcal{H}$ and the reduced optical distance τ.

The clear aperture radius requirement associated with any axial position in the optical system is represented on the Y-$\bar{Y}$ diagram by the quantity $|y| + |\bar{y}|$ at that point.

A list of basic terms and equations pertaining to the Y-$\bar{Y}$ diagram appears in Appendix B. A more detailed treatment of the Y-$\bar{Y}$ diagram is given by Shack (1973).

Vander Lugt Notation

Vander Lugt's operational notation represents the optical system by a block diagram as shown in Fig. 3.2.

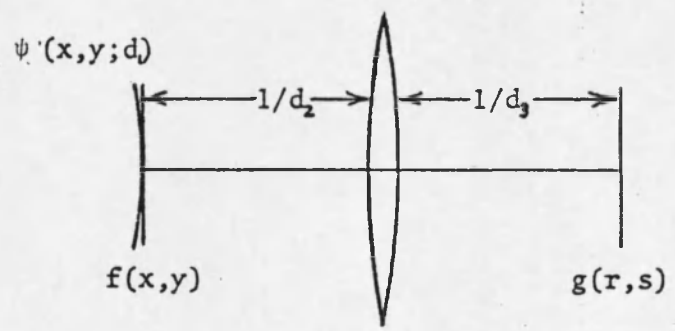

(a)

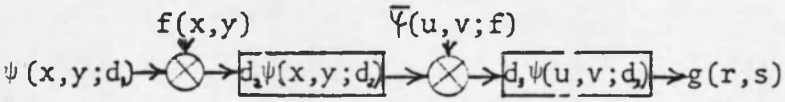

(b)

Fig. 3.2. A single element.

(a) optical system
(b) block diagram

The operations of propagation and lens modification of the wavefront have been reduced to either multiplication by or convolution with a quadratic-type term. The operation of the lens is shown in Fig. 3.3 and is represented by a multiplicative factor $e^{-i\ k/2F\ (x^2+y^2)}$.

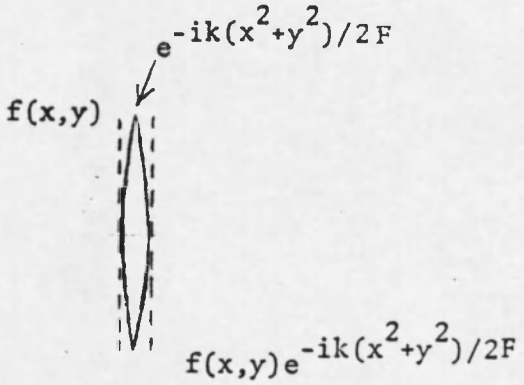

(a)

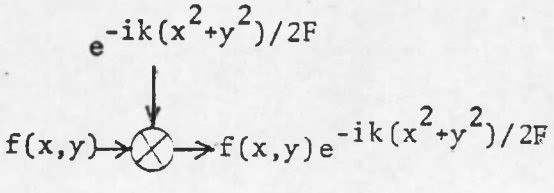

(b)

Fig. 3.3. Lens operation.

(a) optical system
(b) block diagram

Free space can be represented by a device with impulse response $\frac{1}{D} e^{i\, K/2D\ (x^2+y^2)}$ if f(x,y) is the light distribution in a given plane, then the propagated light distribution a distance D from the plane is

$$g(u,v) = \frac{C}{D} \int_{-\infty}^{\infty} f(x,y)\ e^{i\, K/2D[(x-u)^2 + (y-v)^2]}\ dxdy$$

where u,v are coordinates in the new plane and c is a constant (see Fig. 3.4).

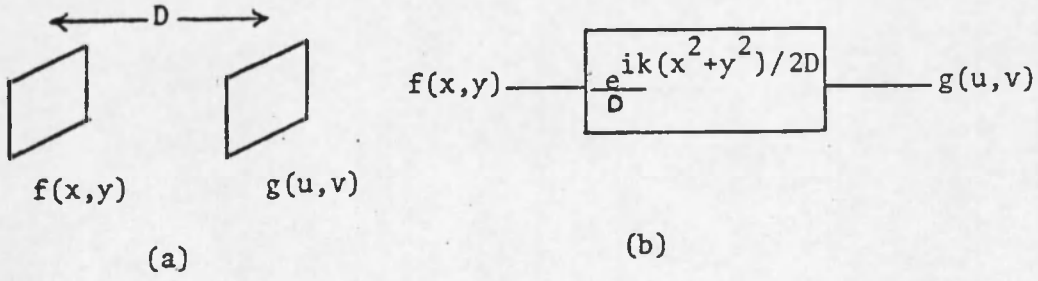

Fig. 3.4. Propagation operation.

(a) optical system
(b) block diagram

To simplify notation, lower case letters represent reciprocal distance $\left(D = \frac{1}{d}\ ,\ F = \frac{1}{f}\right)$ and the function ψ is defined as

$$\psi(x,y;f) \equiv e^{i\ kf/2(x^2+y^2)}$$

with $\overline{\psi}(x,y;f)$ representing the complex conjugate. Using this notation the system represented in Fig. 3.2 can be written as

$$g(r,s) = d_2 d_3 \iint_{P_1} \iint_{P_2} \psi(x,y;d_1) f(x,y) \psi(x-u,y-v;d_2) \overline{\psi}(u,v;f) \psi(u-r,v-s;d_3)$$

$$dxdydudv\ .$$

For a more detailed treatment one is referred to Vander Lugt's paper (1966).

Basic Examples

To show how both methods are to be applied, a single element lens producing a F.T. will be used as an example. This first configuration is pictured in Fig. 3.5, along with the corresponding Y-$\overline{Y}$ diagram and operational notation. The layout consists of a point source illuminating an object f(x,y) that is outside the front focal point of the lens. The lens forms an image of the illuminating point source in a plane that locates the F.T. $F(\xi',\eta')$ of the object, as shown by the linear system representation. On the Y-$\overline{Y}$ diagram the F.T. of the object is located at the y-axis intersection. The marginal ray represents the maximum spatial frequency component present in the object. The quadratic phase curvature associated with this F.T. is given by

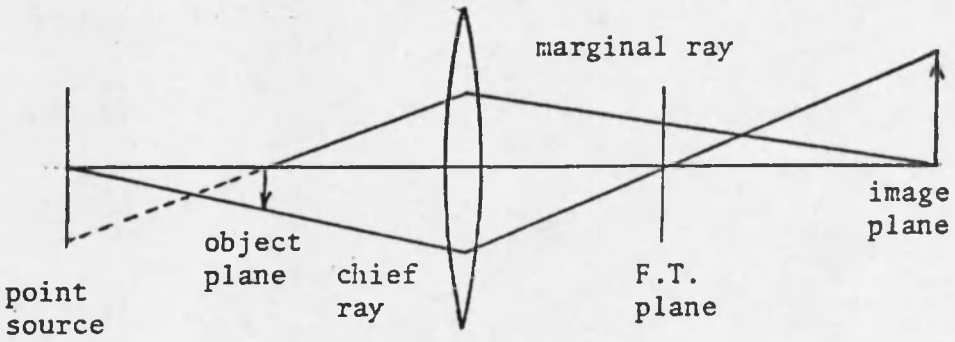

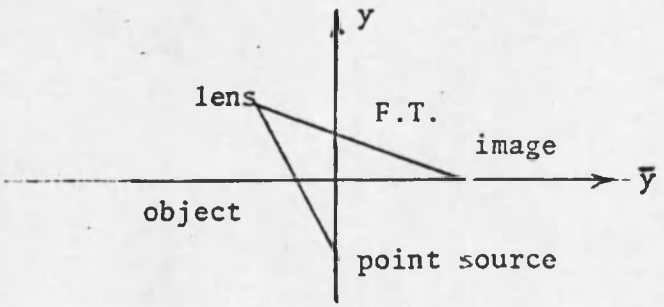

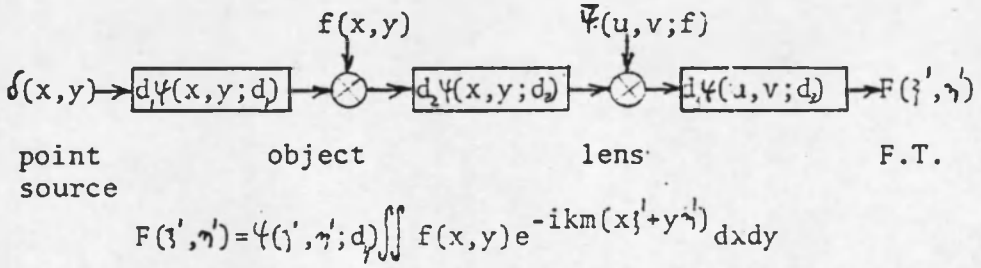

$$F(\xi',\eta') = \psi(\xi',\eta';d_f)\iint f(x,y)\,e^{-ikm(x\xi'+y\eta')}\,dx\,dy$$

Fig. 3.5. Configuration I.

the linear system approach and would be represented on the optical layout as a spherical surface whose center of curvature is located at the final image plane of the object.

Since the Y-$\overline{Y}$ diagram does not contain phase information, comparison of the two systems will be made with respect to intensity. As shown in the last chapter a virtual F.T. exists in the illuminating point source plane (see Fig. 3.6) which may be expressed as

$$|F(\eta)|^2 = \left| \int f(y)\, e^{-i \frac{2\pi}{\lambda} d_1 y \eta}\, dy \right|^2$$

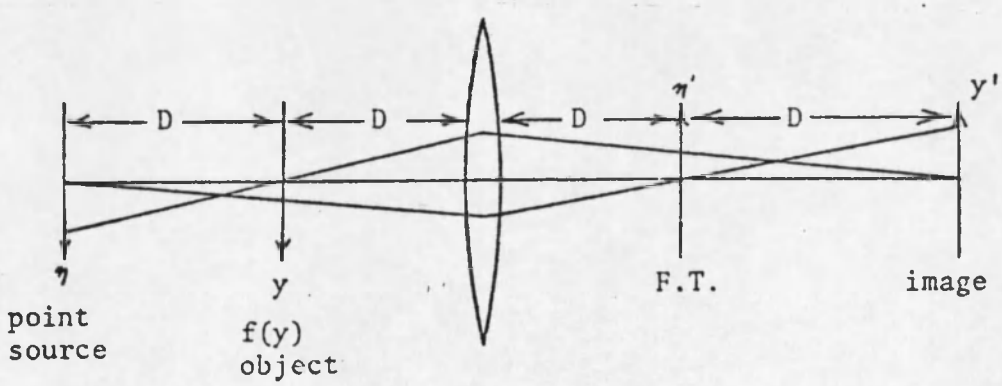

Fig. 3.6. General F.T. optical layout.

This virtual F.T. is then imaged by the lens to form a real F.T. at plane η'. Using the linear systems approach this real F.T. is given by

$$|F(\eta')|^2 = \left| \int f(y)\, e^{-i \frac{2\pi}{\lambda} \frac{(fd_1 + fd_2 - d_1d_2)}{d_2} y\eta'} dy \right|^2 .$$

From Gaussian optics, or from the Y-$\overline{Y}$ diagram, the magnification between these conjugated is known to be

$$m = \frac{D_3}{D_1+D_2} = \frac{d_1d_2}{d_3(d_1+d_2)} = \frac{\eta'}{\eta}$$

$$\eta = \eta' \frac{(fd_1 + fd_2 - d_1d_2)}{d_1d_2} .$$

Substituting this into the virtual F.T. expression gives

$$|F(\eta')|^2 = \left| \int f(y)\, e^{-i \frac{2\pi}{\lambda} \frac{(fd_1 + fd_2 - d_1d_2)}{d_2} y\eta'} dy \right|^2$$

Thus the agreement of the two methods is shown.

If now the object plane is moved to the front focal point of the lens the corresponding system is shown in Fig. 3.7. The quadratic phase factor has now been removed by allowing the image of the object to move to infinity. In Fig. 3.8 the object has been moved inside the focal point of the lens. Note that the sign of the phase curvature has changed, and a virtual image of the object is now present. A final configuration is shown in Fig. 3.9, in which the object has been moved to the other side of the lens. In this case the lens images the illuminating source, but not the object.

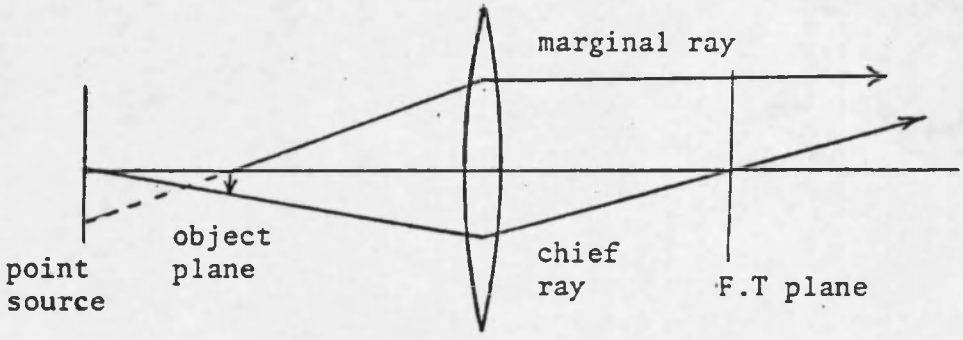

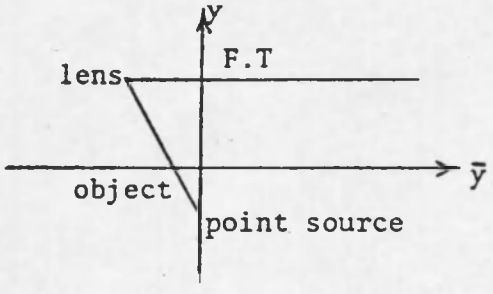

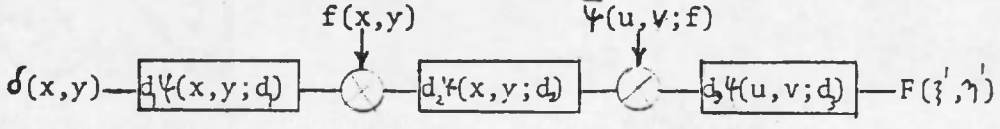

$$F(\xi',\eta')=\iint f(x,y)\,e^{-ikf(x\xi'+y\eta')}\,dxdy$$

Fig. 3.7. Configuration II.

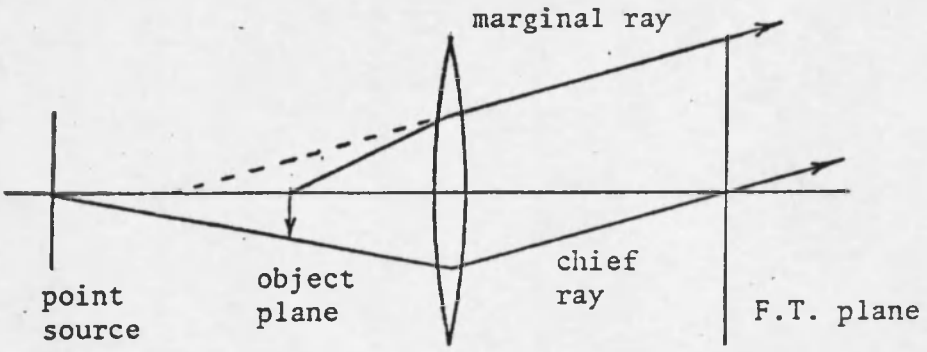

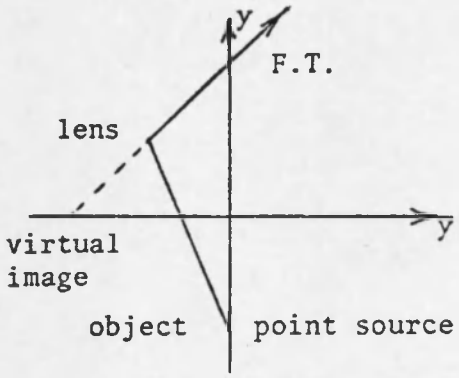

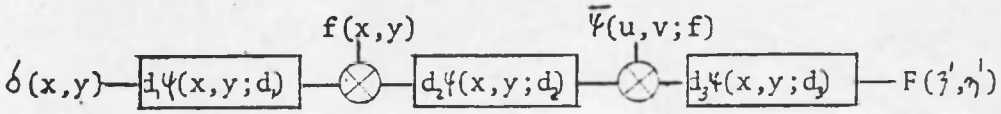

$$F(\xi',\eta') = \Psi(\xi',\eta';d_4)\iint f(x,y)\, e^{-im(x\xi'+y\eta')}\, dxdy$$

Fig. 3.8. Configuration III.

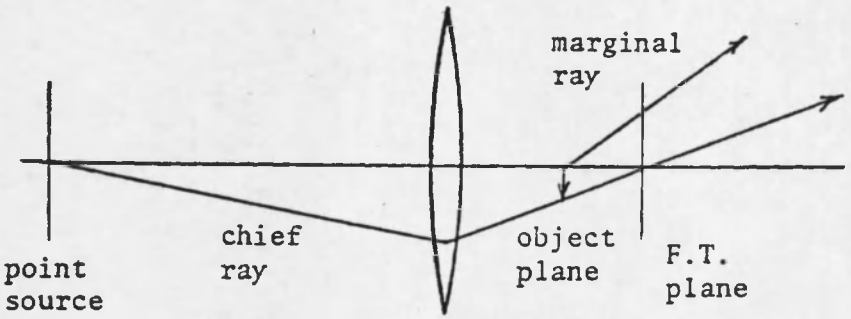

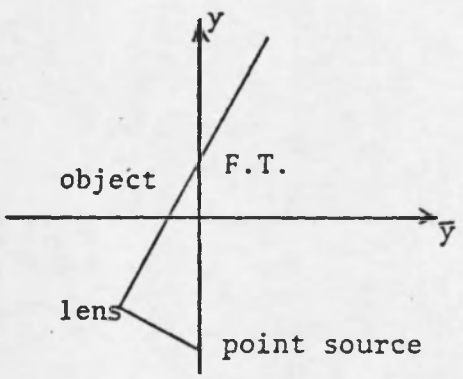

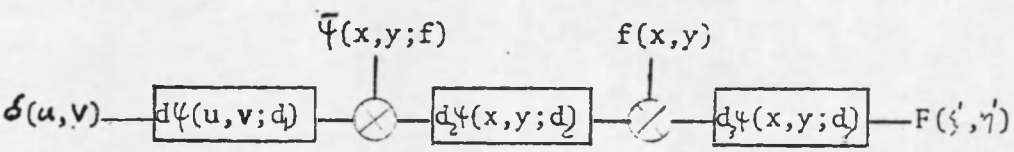

$$F(\xi',\eta') = \psi(\xi',\eta';d_3)\iint f(x,y)\, e^{-ikd_3(x\xi'+y\eta')}\, dxdy$$

Fig. 3.9. Configuration IV.

Reviewing these examples one can see that the bandwidth of a given system is uniquely determined on the Y-$\overline{Y}$ diagram by establishing the clear apertures required of all elements. This is not as apparent in the linear system development.

The Space-bandwidth Product

To further illustrate the Y-$\overline{Y}$ diagram's usefulness let's examine the configuration in Fig. 3.10. This is the common f-f system, and it will be used to demonstrate how the Lagrange invariant, which provides longitudinal scale to the Y-$\overline{Y}$ diagram, is directly related to the space-bandwidth product of the system. The space-bandwidth product is a measure of the complexity of a given function, and represents the number of independent data points contained in the function. The bandwidth of this system is given by

$$\nu_o = \frac{y_2}{\lambda \tau_{12}}$$

and the object width is $2\overline{y}_1$. These form the space-bandwidth product

$$[\nu_o \; 2 \; \overline{y}_1]^2 = \left[\frac{2y_2\overline{y}_1}{\lambda \tau_{12}}\right]^2 .$$

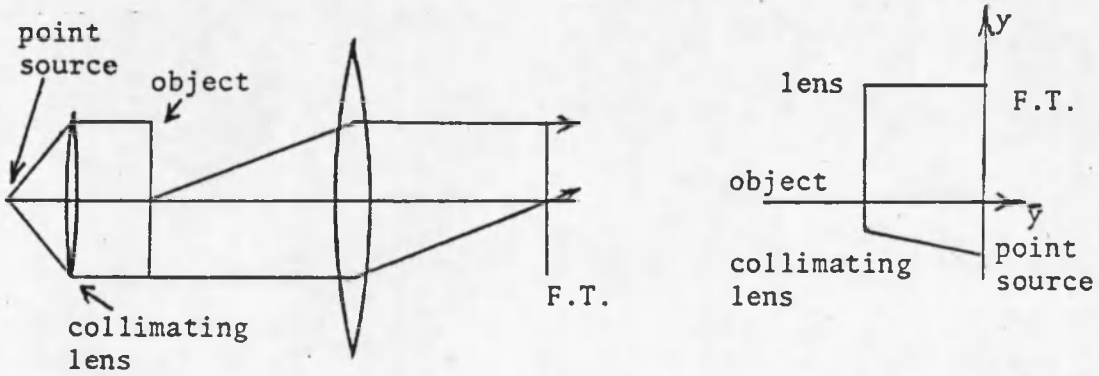

Fig. 3.10. The common "f-f" system.

By substituting $\tau_{12} = \frac{y_2 \bar{y}_1}{\mathscr{H}}$, a basic relationship between the Lagrange invariant and the space-bandwidth product is found.

$$\text{S.B.W.} = \left[\frac{2\,\mathscr{H}}{\lambda}\right]^2$$

In order to obtain the highest possible efficiency in a data-processing system it should be designed to process input functions of the largest possible space-bandwidth product. The Y-$\bar{Y}$ diagram thus allows one to design a system with the space-bandwidth product as an initial parameter. This 1st order representation of the space-bandwidth product can be replaced by an exact expression by making use of the sine condition

$$n'h' \sin U' = n\, h \sin U$$

Using $\mathscr{H} = h\, \bar{y} \sin U$ as an extended Lagrange invariant, and making use of $\nu_o = \frac{\sin U}{\lambda}$, one finds

$$\text{S.B.W.} = [\nu_o\, 2\, \bar{y}_1]^2 = \left[\frac{\sin u}{\lambda}\, 2\, \bar{y}_1\right]^2 = \left[\frac{2\mathscr{H}}{\lambda}\right]^2 .$$

This expression is true for systems that are aplanatic.

Decreasing the Object-F.T. Distance

The Y-$\bar{Y}$ diagram provides valuable insight in the design of a F.T. lens in the attempt to reduce the object-F.T. distance for a given system. To show this use will be made of a normalized Y-$\bar{Y}$ diagram.

The chief ray heights will be divided by the object height and the marginal ray heights divided by the exit pupil height. This means

the Lagrange invariant takes on the value 1/f, where f is the lens focal length. By normalizing the diagram one may separate specific properties, such as F/#, from general ones, including the configuration, and allows a fair comparison of several systems of different parameters. An actual system can be obtained from the normalized Y-$\overline{Y}$ diagram by multiplying the y and $\overline{y}$ values by their appropriate denormalization coefficients, denoted by {}. The relationship between the denormalization coefficients is

$$\{\mathfrak{K}\} = \frac{\{y\}\{\overline{y}\}}{\{\tau\}} = \frac{\{\omega\}\{\overline{\omega}\}}{\{\Phi\}}$$

and when any three values are chosen, the coefficients are all determined.

If one begins with the single element F.T. lens shown in Fig. 3.11a, the object-F.T. distance is 2f. This distance can be reduced while maintaining the 1st order properties of the system by using two elements as shown in Fig. 3.11b. The object-F.T. distance now has been reduced to 1-7/16 f. This distance can be reduced even further by adding a negative element between the two positive elements. A Y-$\overline{Y}$ diagram of this form is shown in Fig. 3.11c. The object-F.T. distance is now 1-1/4 f. These ideas will be used later in the design of complex F.T. lenses in which the object-F.T. distance is to be reduced.

An Actual Design

To show the usefulness of the Y-$\overline{Y}$ diagram in the initial layout of a F.T. system, let's take the example in Fig. 3.11b of two identical

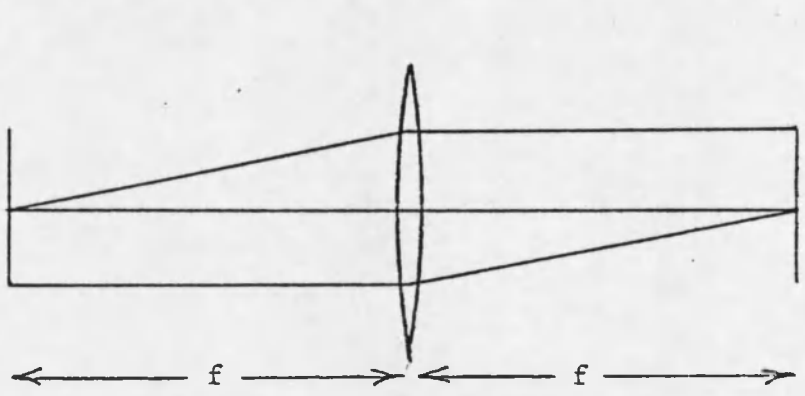

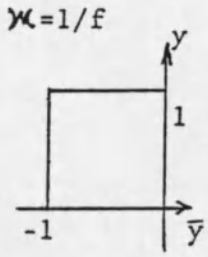

(a) Singlet

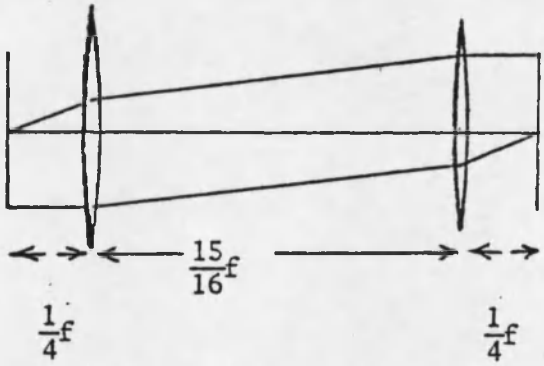

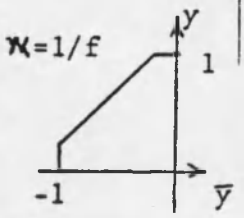

(b) Doublet

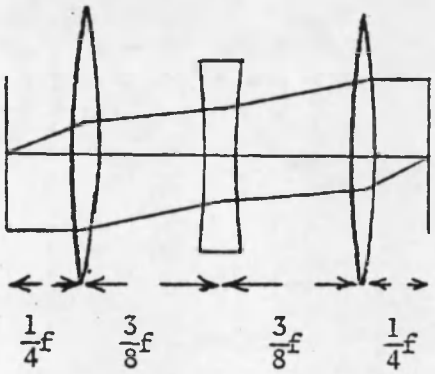

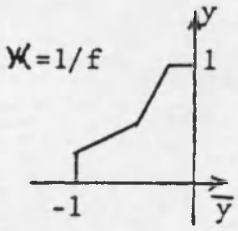

(c) Triplet

Fig. 3.11. Decreasing the object-F.T. distance.

elements that are to be used together to form a F.T. lens. In the lab two lenses of focal length 304.8 mm were available for the exercise. A normalized Y-$\bar{Y}$ layout of two elements will first be developed, as shown in Fig. 3.12.

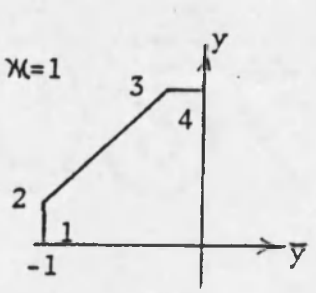

ℋ=1	y	$\bar{y}$	τ	ω	$\bar{\omega}$	ϕ
1	0	-1				
			y_2	1	0	$\frac{1}{1+y_2}$
2	y_2	-1				
			$-y_2^2+1$	$\frac{1}{1+y_2}$	$\frac{1}{1+y_2}$	
3	1	$-y_2$				$\frac{1}{1+y_2}$
			y_2	0	1	
4	1	0				

Fig. 3.12. Normalized system.

The following requirements were chosen.

S.B.W. = 10^5

bandwidth 30 1/mm

input format=output format

If the system is to work at wavelength .6328 μm and the space-bandwidth product is 10^5 the Lagrange invariant has been determined:

$$\mathcal{H} = \frac{\lambda(\text{S.B.W.})^{1/2}}{2} = .1 \quad .$$

A bandwidth of 30 1/mm gives an input format of -5.270 mm. The output format being of the same size the denormalizing coefficient associated with the axial distances must be $\frac{\{y\}^2}{\{\mathcal{H}\}} = 277.626$. An element of focal length 304.8 mm requires that $y_2 = .0979$ on the normalized Y-$\bar{Y}$ diagram. The resulting Y-$\bar{Y}$ diagram is shown in Fig. 3.13.

From this example one can see the value of the Y-$\bar{Y}$ diagram in the initial layout of a F.T. lens. A change in the initial parameters does not require a new Y-$\bar{Y}$ layout, but only a change in denormalization coefficients.

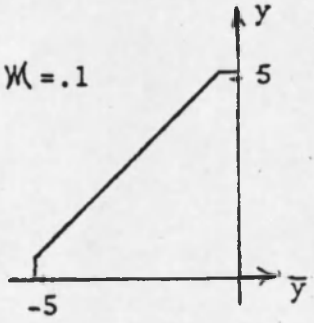

ϰ=.1	y	$\bar{y}$	τ	ω	$\bar{\omega}$	ϕ
1	0	-5.27				
			27.179	.01898	0	
2	.516	-5.27				.00328
			274.965	.01729	.01729	
3	5.27	.516				.00328
			27.179	0	.01898	
4	5.27	0				

object-F.T. distance 329.3 mm f_{eff} 277.6 mm

Fig. 3.13. Denormalized system.

CHAPTER 4

SIMPLE F.T. LENSES

In this chapter simple F.T. lenses are defined and their limitations investigated. All designs will be done for f-f systems since these have no phase curvature in the F.T. plane and are thus of practical importance. Simple F.T. lenses are classified as those whose object-F.T. distance is ~2f. The Y-$\bar{Y}$ diagram representation of these lenses is shown in Fig. 4.1. The F.T. lens in represented as point #2 on the diagram while the object and the F.T. correspond to points #1 and #3.

Two different approaches can be taken in the design of simple F.T. lenses. The first is the use of a symmetrical system. This method will not work if a cemented doublet is to be used. The second approach is to design the lens such that it is optimized at the required two sets of conjugates. This can be done using a lens design

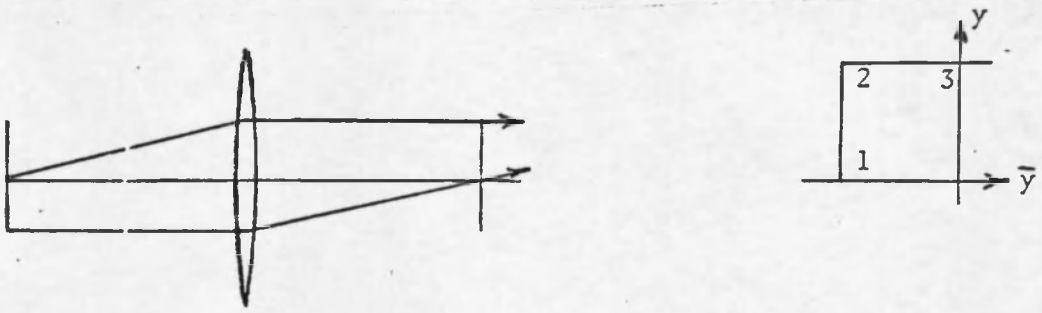

Fig. 4.1. Y-$\bar{Y}$ diagram of simple F.T. lens.

program that allows optimization simultaneously at different conjugates (multi-configuration optimization) or by designing the lens at magnification -1 (m=-1) and knowing the relationship between this imagery and that at the desired conjugates m=0 and m=∞. Such a method was used by Wynne (1974) in the design of F.T. lenses.

Wynne's approach was to design the lens at magnification -1, with the stop at the element, by correcting for spherical aberration and coma. This method only works if all surfaces of the elements are very near the stop in the m=-1 configuration, which restricts its use to contact and cemented thin lenses. By using the conjugate and stop shift formulae one can determine the final object and pupil aberrations in terms of the m=-1 configuration aberrations and with the proper choice of the m=-1 configuration aberrations a reasonable final result can be obtained. This method will be used to design a set of singlet and doublet lenses.

Design Method

The starting point for this set of designs is the relationship between the imagery of the different conjugates. Use will be made of Shack's structural aberration coefficients (1974) in deriving the desired relationships. The system will be designed in the configuration pictured in Fig. 4.2. The m=0 imagery (Fig. 4.3) and the m=∞ imagery (Fig. 4.4) are the two configurations of interest. The desired relationship is one that relates the m=-1 imagery to the m=0 and m=∞ imagery. This is found by making use of the conjugate shift and stop shift formulae described in Appendix A and listed below.

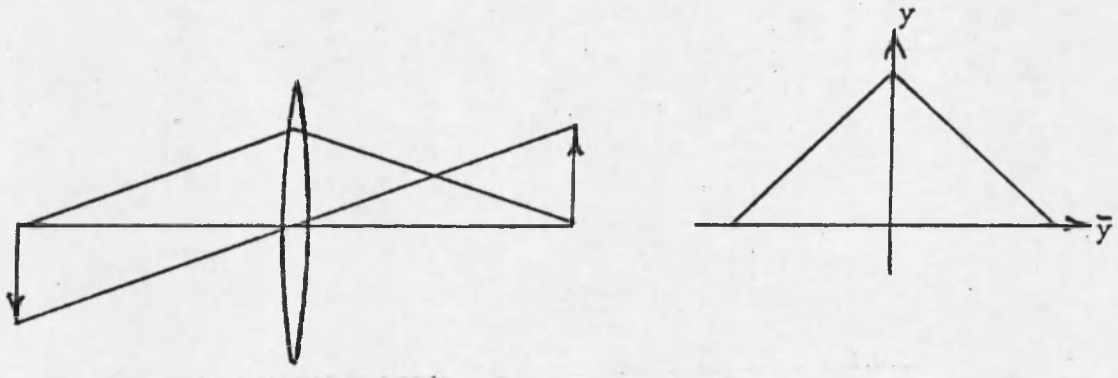

Fig. 4.2. Basic design configuration m=-1.

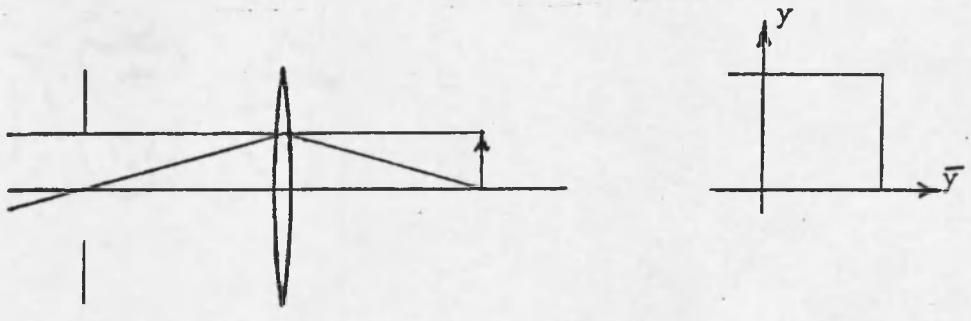

Fig. 4.3. m=0 imagery.

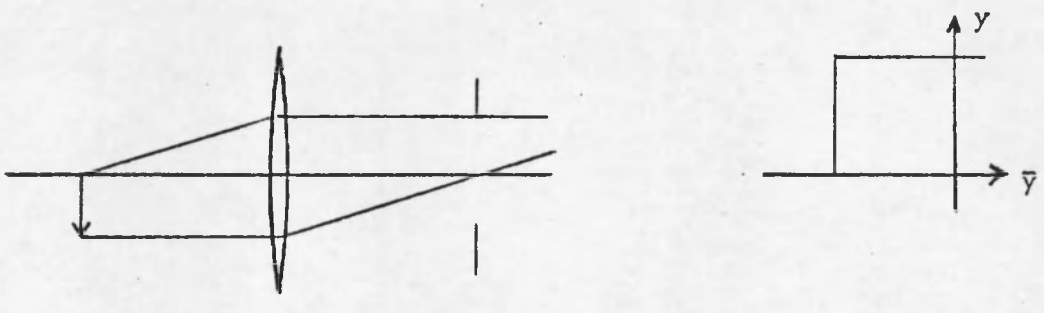

Fig. 4.4. m=∞ imagery.

Conjugate shift formulae (shift from Y=0 conjugate):

$$\sigma_I^* = \sigma_I - (3\sigma_{II} + \bar{\sigma}_V)Y + (3\sigma_{III} + 2\sigma_{IV} + 3\bar{\sigma}_{III})Y^2 - (\sigma_V + 3\bar{\sigma}_{II})Y^3 + \bar{\sigma}_I Y^4$$

$$\sigma_{II}^* = \sigma_{II} - (2\sigma_{III} + \sigma_{IV} + \bar{\sigma}_{III})Y + (\sigma_V + 2\bar{\sigma}_{II})Y^2 - \bar{\sigma}_I Y^3$$

$$\sigma_{III}^* = \sigma_{III} - (\sigma_V + \bar{\sigma}_{II})Y + \bar{\sigma}_I Y^2$$

$$\sigma_{IV}^* = \sigma_{IV}$$

$$\sigma_V^* = \sigma_V - \bar{\sigma}_I Y$$

Stop shift formulae:

$$\sigma_I' = \sigma_I$$

$$\sigma_{II}' = \sigma_{II} + \sigma_I S$$

$$\sigma_{III}' = \sigma_{III} + 2\sigma_{II}S + \sigma_I S^2$$

$$\sigma_{IV}' = \sigma_{IV}$$

$$\sigma_V' = \sigma_V + (\sigma_{IV} + 3\sigma_{III})S + 3\sigma_{II}S^2 + \sigma_I S^3$$

The conjugate shift formulae can be simplified by the fact that for the m=-1 configuration specified (i.e., all elements at the stop), the pupil aberrations are

$$\bar{\sigma}_I = 0 \qquad \bar{\sigma}_{IV} = \sigma_{IV}$$

$$\bar{\sigma}_{II} = 0 \qquad \sigma_V = \sigma_{II}$$

$$\bar{\sigma}_{III} = 0$$

Using these values for the m=-1 configuration and applying the conjugate and stop shift formulae in succession to the m=-1 configuration the following dependence of the m=∞ and m=0 primary aberrations on the m=-1 configuration are found.

m=∞	m=0
$\bar{\sigma}_I^{**} = \sigma_I - 4\sigma_{II} + 3\sigma_{III} + 2\sigma_{IV}$	$\sigma_I^{**} = \sigma_I + 4\sigma_{II} + 3\sigma_{III} + 2\sigma_{IV}$
$\bar{\sigma}_{II}^{**} = \frac{1}{2}\sigma_I - \sigma_{II} - \frac{1}{2}\sigma_{III}$	$\sigma_{II}^{**} = -\frac{1}{2}\sigma_I - \sigma_{II} + \frac{1}{2}\sigma_{III}$
$\bar{\sigma}_{III}^{**} = \frac{1}{4}\sigma_I - \frac{1}{4}\sigma_{III} - \frac{1}{2}\sigma_{IV}$	$\sigma_{III}^{**} = \frac{1}{4}\sigma_I - \frac{1}{4}\sigma_{III} - \frac{1}{2}\sigma_{IV}$
$\bar{\sigma}_{IV}^{**} = \sigma_{IV}$	$\sigma_{IV}^{**} = \sigma_{IV}$
$\bar{\sigma}_V^{**} = \frac{1}{8}\sigma_I + \frac{1}{4}\sigma_{II} + \frac{3}{8}\sigma_{III}$	$\sigma_V^{**} = -\frac{1}{8}\sigma_I + \frac{1}{4}\sigma_{II} - \frac{3}{8}\sigma_{III}$

If the two conditions $\sigma_{II} = 0$ and $\sigma_I = \sigma_{III} = 1$ are placed on the m=-1 configuration, medial focus ($\sigma_{IV}^{**} = -2\sigma_{III}^{**}$) is achieved for the m=0 conjugate, and if the input and output formats are of the same size, the following is true for the m=∞ and m=0 aberrations:

$$\bar{S}_I^{**} = S_I^{**}$$

$$\bar{S}_{II}^{**} = S_{II}^{**} = 0$$

$$\bar{S}_{III}^{**} = S_{III}^{**}$$

$$\bar{S}_{IV}^{**} = S_{IV}^{**}$$

$$\bar{S}_V^{**} = S_V^{**}$$

For a single element F.T. lens the requirements mentioned above for the m=-1 configuration become X=0 and σ_I=1 which gives the following aberrations:

$$W_{040} = \frac{1}{8}\left(1 + \frac{1}{2n}\right)\phi^3 h^4$$

$$W_{131} = 0$$

$$W_{222} = -\frac{\phi^3 h^4}{4n}$$

$$W_{220p} = \frac{\phi^3 h^4}{4n}$$

$$W_{311} = \frac{\phi^3 h^4}{2} = \frac{\mathcal{H}\,\Delta(\bar{u}^2)}{2}$$

Let's look at the following single element.

Example 1 Glass: LaSF5

n_d = 1.880692

h = 30 mm

$W_{040} = 2.1814 \times 10^8\ 1/f$ waves

$W_{131} = 0$

$W_{222} = -1.8325 \times 10^8\ 1/f^3$

$W_{220p} = 1.8325 \times 10^8\ 1/f^3$

$W_{311} = 6.8929 \times 10^8\ 1/f^3$

A graph of these results is shown in Fig. 4.5.

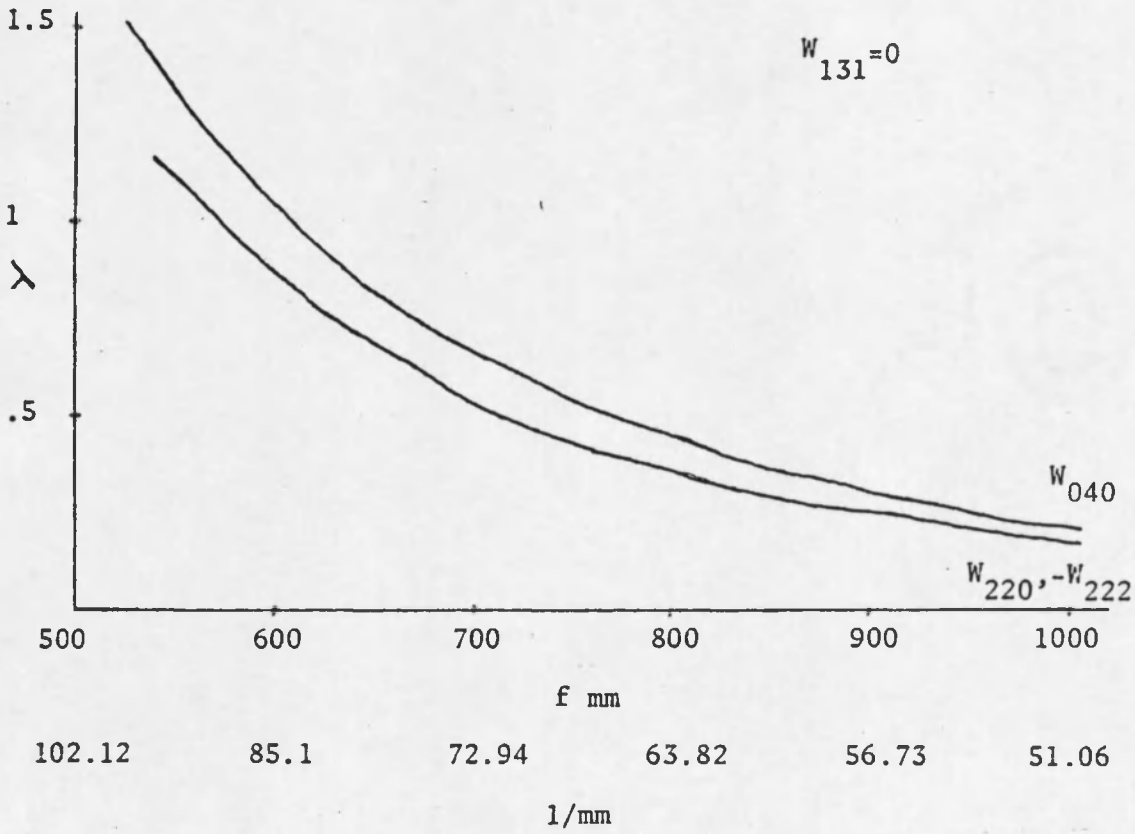

Fig. 4.5. Single element example I.

A different choice of aberration balance could be a flat tangential field ($\sigma^{**}_{IV} = -3\sigma^{**}_{III}$). For the single lens element it is required that X=0, and $\sigma_I = 1 + \frac{2}{3n}$ which gives

$$W_{040} = \frac{1}{8}\left[1 + \frac{2}{3n}\right]\phi^3 h^4$$

$$W_{131} = \frac{-1}{12n}\ \phi^3 h^4$$

$$W_{222} = \frac{1}{6n}\,\phi^3 h^4$$

$$W_{220p} = \frac{1}{4n}\,\phi^3 h^4$$

$$W_{311} = \frac{1}{2}\left[1 + \frac{1}{6n}\right]\phi^3 h^4$$

Using example I parameters again we find (Fig. 4.6):

$$W_{040} = 2.334 \times 10^{8}\ 1/f^{3} \text{ waves}$$

$$W_{131} = 6.1085 \times 10^{8}\ 1/f^{3}$$

$$W_{222} = -1.2217 \times 10^{8}\ 1/f^{3}$$

$$W_{220_P} = 1.8325 \times 10^{8}\ 1/f^{3}$$

$$W_{311} = 7.5038 \times 10^{8}\ 1/f^{3}$$

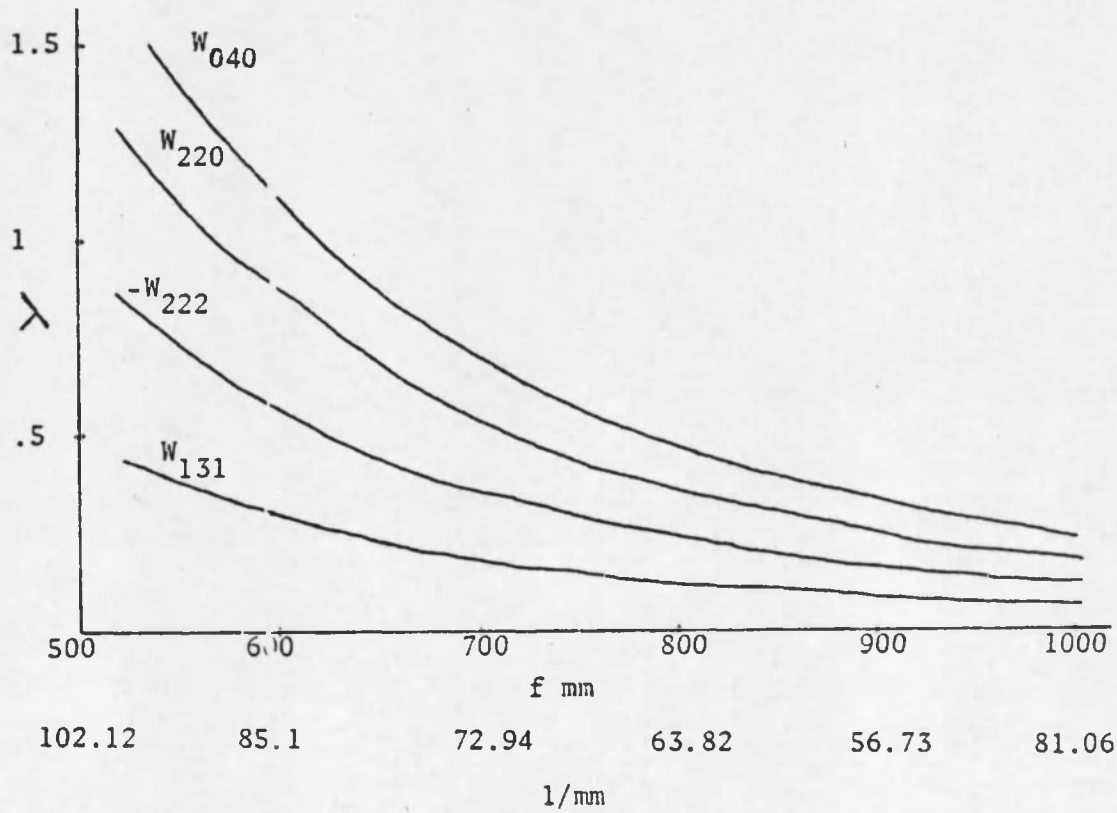

Fig. 4.6. Single element flat tangential field.

It is seen in this case that the reduction in astigmatism was accomplished at the expense of coma and spherical aberration.

Designs

For the design examples to follow let's use the 1st case as the desired imagery and try to make the system as short as possible. Let's choose f=600 mm which means spherical is $\sim 1\lambda$. Thus for an input format of 60 mm this will be an f/10 system. A 60 mm output format gives a maximum spatial frequency of 85.1 1/mm.

Aspheric Singlet

For this design no computer optimization was actually required since the proper aspheric can be calculated to give the correct amount of spherical aberration. The requirements of the system at Y=0 conjugate are $\sigma_{II}=0$ and $\sigma_I=\sigma_{III}=1$. The $\sigma_I=0$ requirement is satisfied by choosing the proper aspheric for the surface. These considerations led to the following design listed in Table 4.1

Table 4.1. Aspheric singlet design.

SURFACE	CURVATURE	THICKNESS	GLASS
1	.000948	9.3	LaSF5
2	-.000948*		

* conic constant -5.522768 UNITS MM

FRONT FOCAL DISTANCE 597.522 mm

The wavefront rms error for this lens as a function of spatial frequency is shown in Fig. 4.7. The value of distortion was -.124%, with the desired value being -.125% which can be obtained by using the formula

$$S_V = -\mathcal{H} \Delta(\bar{u}^2) \ .$$

On turning the lens around and evaluating the imagery for the other set of conjugates it was found to be almost identical.

Cemented Doublet

If one chooses not to use aspherics in the design, then a second element must be added so the proper target value for σ_I can be obtained. Thus a cemented doublet was the obvious next choice for the design. In this case the lens had to be optimized using the ACCOSV lens design program. Optimizing the lens at Y=0 conjugates and target values for SA3 of -.01875 and CMA3 of 0 resulted in the design listed in Table 4.2.

Table 4.2. Cemented doublet.

SURFACE	CURVATURE	THICKNESS	GLASS
1	.001013	20	BaSF51
2	-.005021	12	LaK17
3	-.00159		

FRONT FOCAL DISTANCE 594 MM

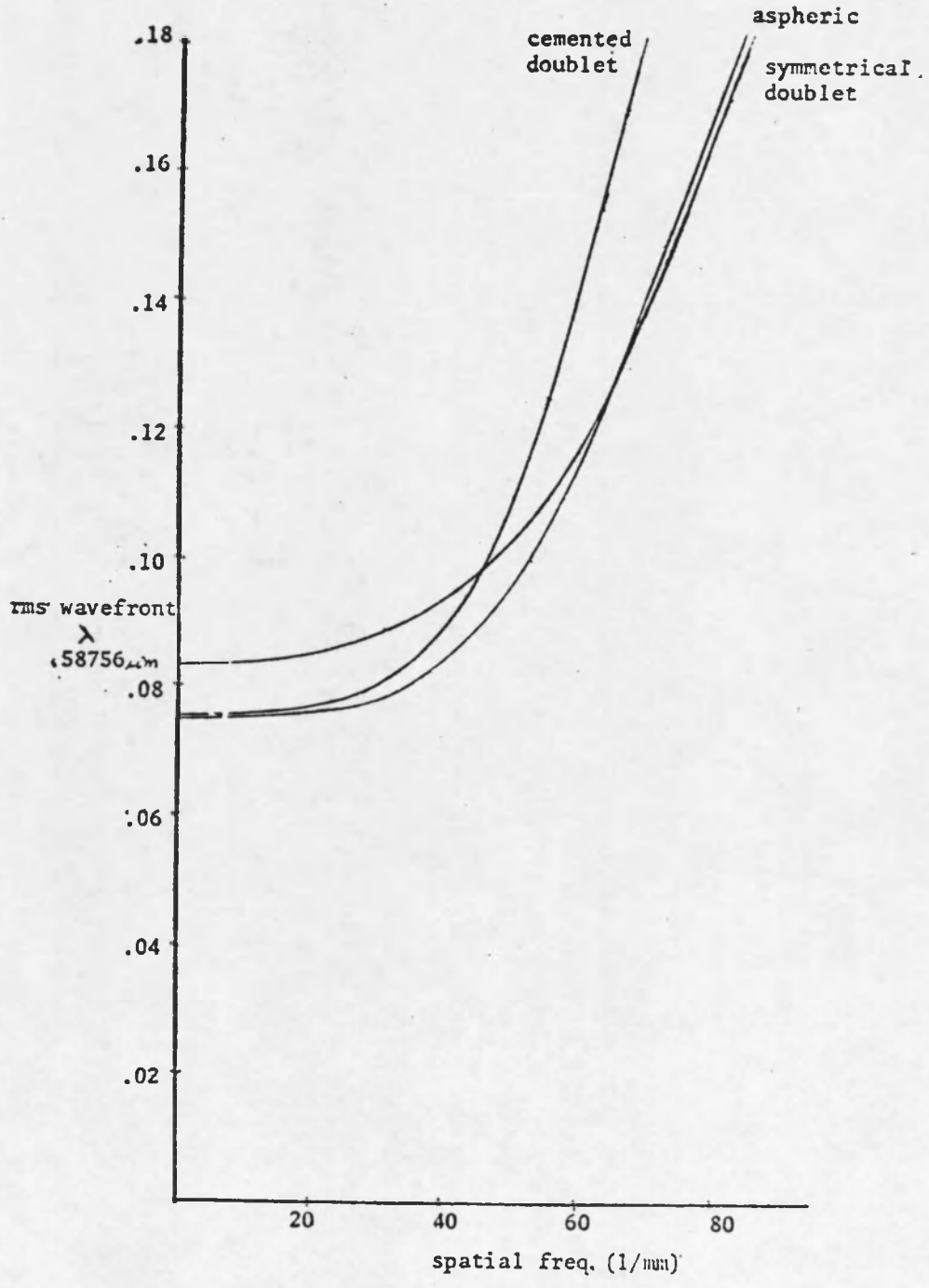

Fig. 4.7. Wavefront rms error vs. spatial frequency for simple F.T. lenses.

The wavefront rms error versus spatial frequency of this lens is shown in Fig. 4.7. The distortion present is -.1255%. On turning the lens around, the second set of conjugates gave identical imagery.

A non-cemented doublet was designed using the method of these first two designs and its imagery was found to be similar to that of the cemented doublet.

Symmetrical Doublet

For this last design the symmetry principle was used. In this design the lens will be optimized at m=0 conjugate, with the stop at the front focal point and symmetry maintained such that the m=∞ conjugate aberrations are identical to the m=0 conjugate aberrations. The optimized design is listed in Table 4.3. The distortion value was -.1327%, and the wavefront rms error is shown in Fig. 4.7.

Table 4.3. Symmetrical doublet.

SURFACE	CURVATURE	DISTANCE	GLASS
1	.000077	9.95381	LaK17
2	-.000981		
3	.000981	0	
4	-.000077	9.95381	LaK17

CHAPTER 5

COMPLEX F.T. LENSES

Complex F.T. lenses will be dealt with in this chapter and how they can be used in decreasing the object-F.T. distance while improving the F.T. imagery quality over the simple F.T. lenses of the last chapter.

A complex F.T. lens will simply be classified as any lens that does not meet the requirements of being a simple F.T. lens. Any element separated from the stop leaves the conjugate shift formulae in a very complex form so that little can be gained from their use beyond the simple F.T. lens case. The problem stems from the fact that all the pupil aberrations of the initial system now have finite values. Another possible problem with this method is that it only takes into account the 3rd order aberrations, although higher orders for complex F.T. lenses will be of importance in their design. Thus for the design of this group of lenses, use will be made of the symmetry principle. Both the object and pupil imagery must be corrected, but only one set of conjugates need be considered in the symmetrical design. A break from this symmetry condition would require looking at both sets of conjugates and it is not clear that this would provide much in the way of improving the design.

The need for the complex designs is to improve the imagery by increasing the number of degrees of freedom available for aberration

control while also reducing the object-F.T. distance. To reduce the system's overall length the principal planes are crossed.

Use was made of the Y-$\overline{Y}$ diagram in the pre-design of each one of these lenses. The same system parameters as for the simple F.T. lenses will be used, i.e., f=600 mm and input and output formats of 60 mm. No attempt will be made at a mathematical solution except in reducing the initial Petzval curvature. A mathematical approach was examined by Blandford (1970).

The design objective will be to minimize the amount of spherical aberration, coma and astigmatism to obtain the best imagery possible. Field curvature will not be considered as important in these designs. This is just one possible design scheme one may follow. Other possibilities could be a flat tangential or flat medial field.

Design Scheme

The initial system to be optimized was arrived at by making use of the Y-$\overline{Y}$ diagram. With the requirement that Petzval curvature be zero, a distribution of the power between the thin lens elements can be found. Indexes were chosen to help in the initial reduction of the Petzval sum. The initial axial distances where chosen to reduce the object-F.T. distance to approximately 700 mm. The shape factors of the elements were determined by first making a reasonable guess and then evaluating the results using a Y-$\overline{Y}$ computer program developed by Shack (1979). After a few adjustments of the shape factors of the elements a reasonable starting point was found. The lens was then optimized using the ACCOSV lens design program (ACCOSV, 1971).

The basic idea behind the optimization routine was to maintain the 1st order constraints and the symmetry while varying the surface curvatures and axial distances to reduce the aberrations. A triplet lens will be used to show the basic optimization routine ideas (see Fig. 5.1). The symmetry of the system was maintained by using the pickup command in ACCOSV. The first half of the lenses parameters (curvatures, thicknesses, indexes) are used as variables while the second half parameters are picked up from the first half. The 1st order constraints (focal length, telecentricity, f/#) were maintained by forcing the marginal ray to be zero at the final distance (t_1' in Fig. 5.1) and requiring the chief ray height at this surface to be equal to that of the marginal ray at the entrance pupil.

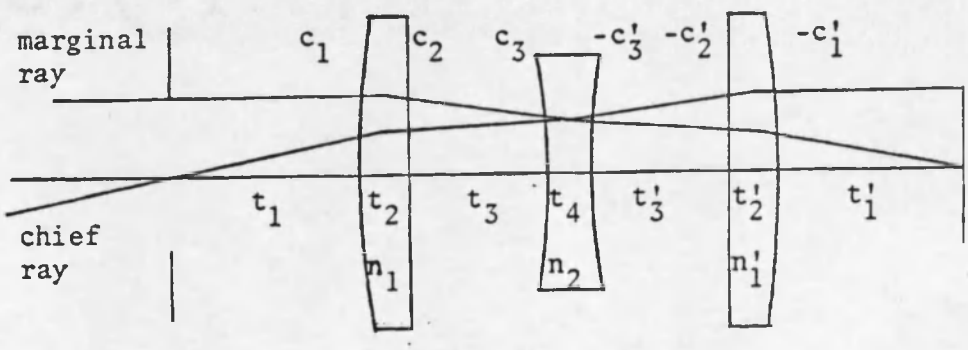

Fig. 5.1. Optimization routine example.

Complex F.T. Lens Designs

The first design is made up of two elements and is shown in the Y-$\overline{Y}$ diagram of Fig. 5.2. The basic system data is listed in Table 5.1.

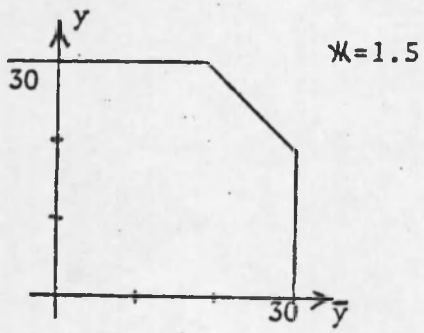

Fig. 5.2. Symmetrical doublet.

Table 5.1. Basic lens data for the symmetrical doublet.

SURFACE	CURVATURE	THICKNESS	GLASS
1	.000435	10	LaK17
2	-.000893	384.83	
3	.000893	10	LaK17
4	-.000435		

OBJECT-F.T. DISTANCE 1100 mm

FRONT FOCAL DISTANCE 352.47 mm

The amount of distortion present in the design is -.1276% (the target value was -.125%). In Fig. 5.3 the rms wavefront versus spatial frequency is plotted for various focal positions. This allows one to choose best focus for a given rms wavefront tolerance and determine the maximum spatial frequency allowable to meet this requirement.

The second design is a symmetrical triplet and the Y-$\overline{Y}$ diagram is shown in Fig. 5.4. The basic system data is listed in Table 5.2. The distortion for this design was -.1209%. The rms wavefront error versus spatial frequency plot is shown in Fig. 5.5.

The final design is a 4-element one. Its Y=$\overline{Y}$ diagram is shown in Fig. 5.6. The basic system data is listed in Table 5.3. The value of distortion for this lens is -.1241%. The wavefront rms error versus spatial frequency plot for this design is shown in Fig. 5.7.

Other designs could be done by adding more elements, i.e., five- and six-element designs, thus allowing one to reduce the object-F.T. distance even more. Harris (1975) created an outstanding six-element design that is diffraction-limited with the specification listed below.

wavelength -500 nm

EFL -1000 mm

object diameter -150 mm(f/6.67)

aperture stop diameter -150 mm(150 1/mm)

object-F.T. distance -814.8 mm.

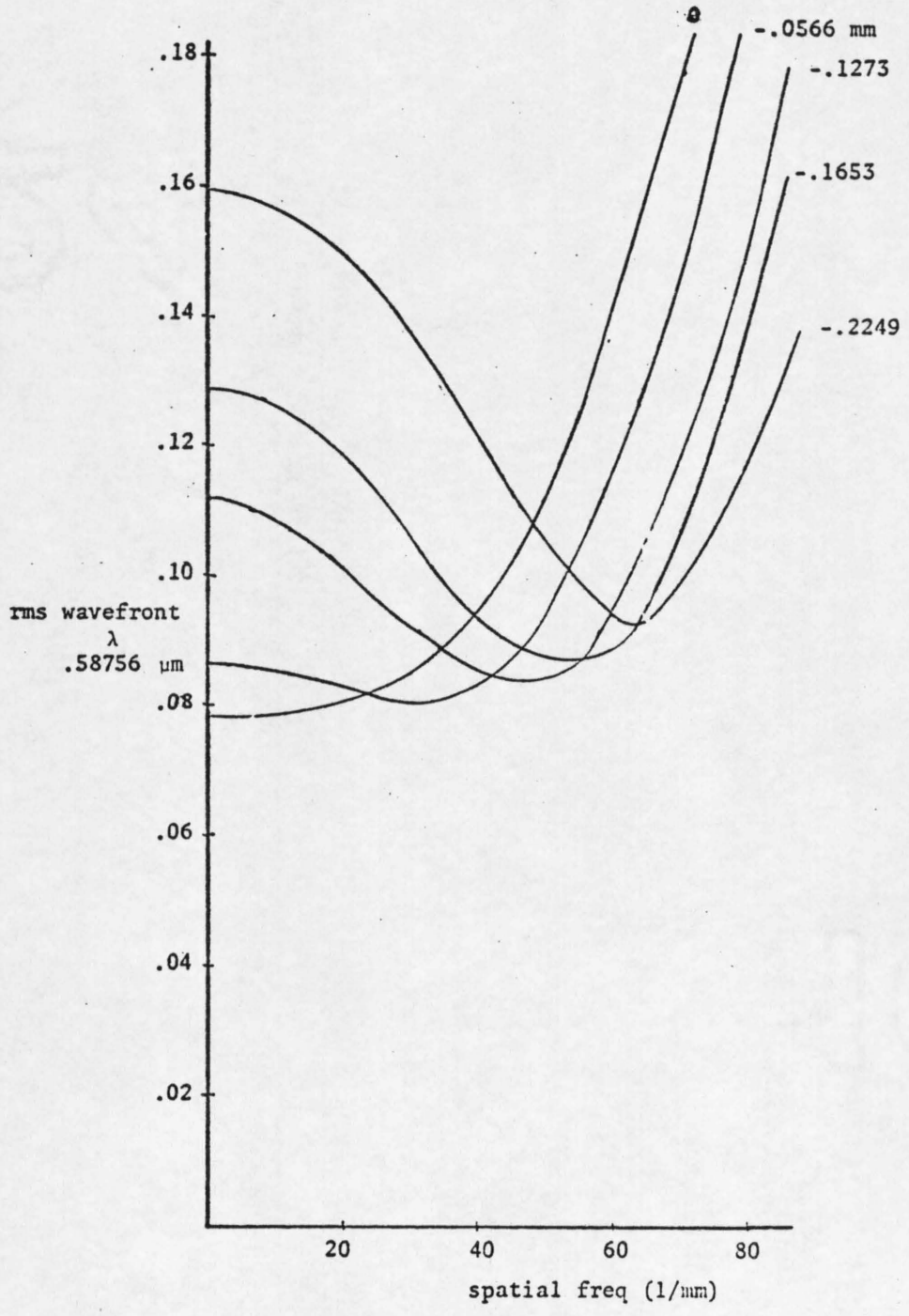

Fig. 5.3. RMS wavefront error for the symmetrical doublet at several focus positions.

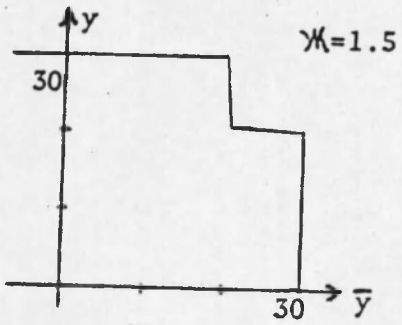

Fig. 5.4. Symmetrical triplet.

Table 5.2. Basic lens data for the symmetrical triplet design.

SURFACE	CURVATURE	THICKNESS	GLASS
1	.001769	18	LaK17
2	-.00103	127.51	
3	-.002733	10	K50
4	.002733	127.51	
5	.00103	18	LaK17
6	-.001769		
	OBJECT-F.T DISTANCE	1100 mm	
	FRONT FOCAL DISTANCE	400 mm	

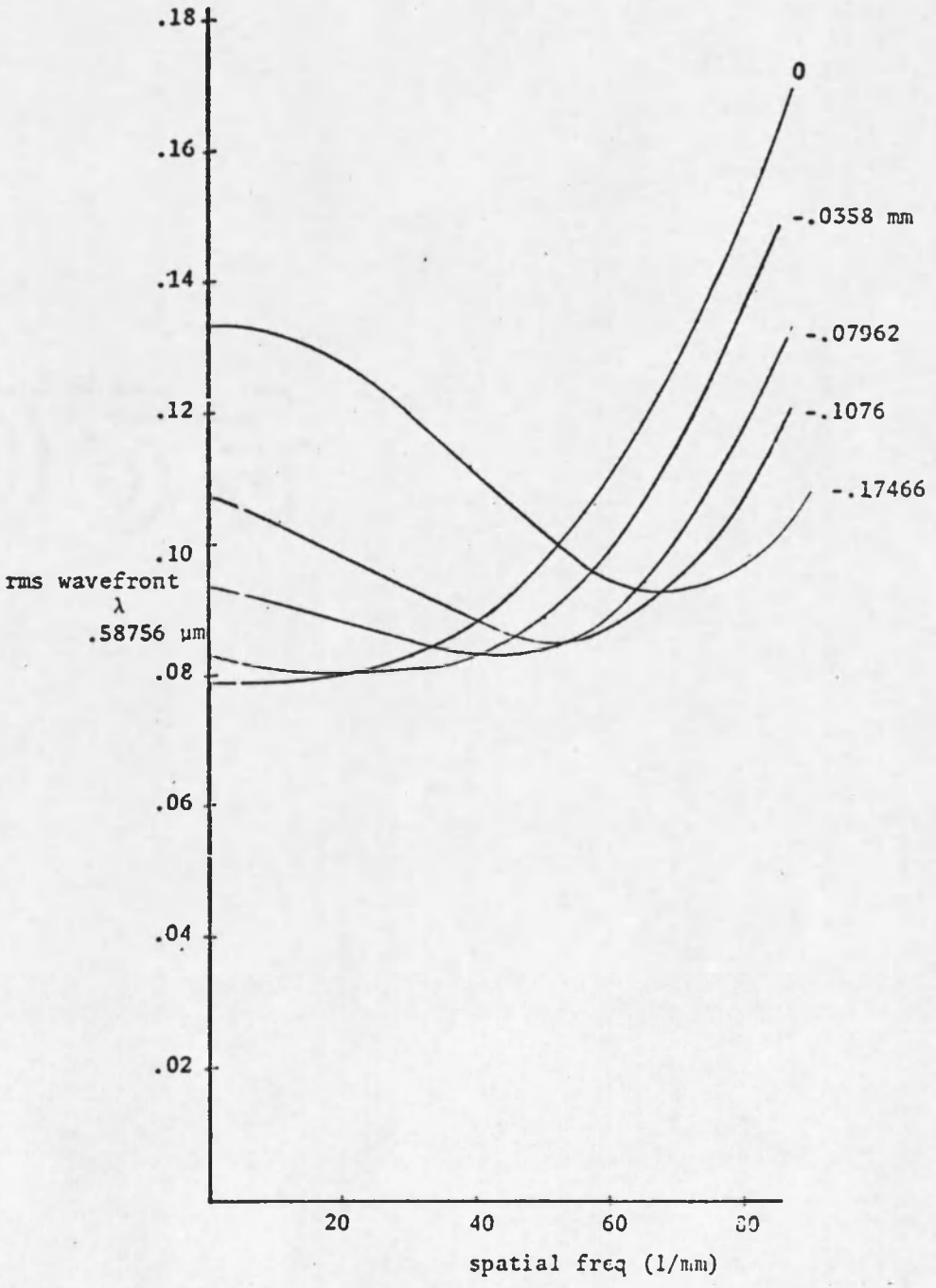

Fig. 5.5. RMS wavefront error for the symmetrical triplet at several focus positions.

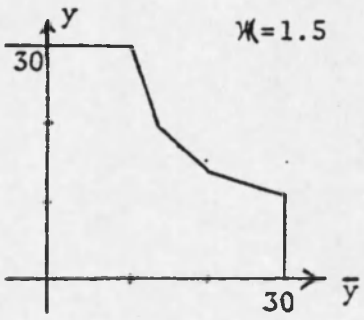

Fig. 5.6. Symmetrical 4-element.

Table 5.3. Basic lens data for symmetrical 4-element design.

SURFACE	CURVATURE	THICKNESS	GLASS
1	.004709	25	LaF13
2	.001866	111.302	
3	.006402	8.42	K50
4	.008975	136.81	
5	-.008975	8.42	K50
6	-.006402	111.302	
7	-.001866	25	LaF13
8	-.004709		
	OBJECT-F.T. DISTANCE	850 mm	
	FRONT FOCAL DISTANCE	225 mm	

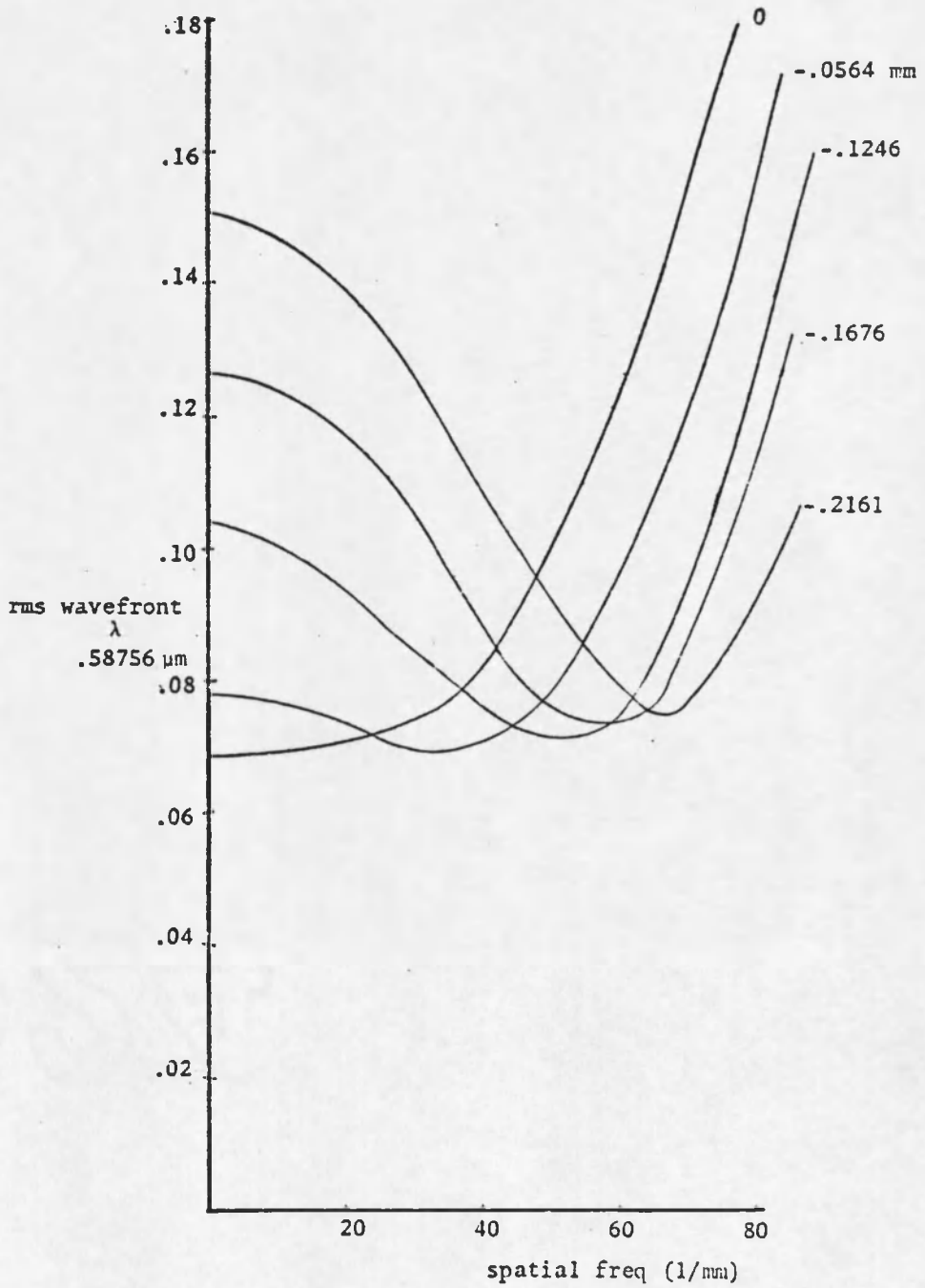

Fig. 5.7. RMS wavefront error for the symmetrical 4-element design at several focus positions.

CHAPTER 6

CONCLUSION

A clearer understanding of coherent imaging systems has been gained in dealing with the design of F.T. lenses. It was found that Gaussian optics could be used in only one specific case, the f-f system, to meaningfully discuss a coherent system. A general discussion has to be done in the Sine ideal representation of image formation, which allows the calculation of piston error.

The quantity S_{VI} was found to differ from that of previous works (Wynne, 1952), and an example was given to justify its current representation. It was shown that this new representation of S_{VI} does not change the conjugate shift formulae which were used in the design of simple F.T. lens examples.

Further work could be done on the design of F.T. elements in looking at anamorphic lens systems, which are used in multi-channel data-processing systems. Another area of future research could be in the design of holographic F.T. elements.

APPENDIX A

CONJUGATE SHIFT AND STOP SHIFT FORMULAE

This appendix lists the set of conjugate shift and stop shift formulae for the third order aberrations. They are used in Chapter 3 in the design of simple F.T. lenses.

The stop shift functional dependence can be found in several texts (e.g., Welford, 1974). They are listed below.

$$
\begin{aligned}
S_I' &= S_I \\
S_{II}' &= S_{II} + \left(\frac{\delta\bar{y}}{y}\right) S_I \\
S_{III}' &= S_{III} + 2\left(\frac{\delta\bar{y}}{y}\right) S_{II} + \left(\frac{\delta\bar{y}}{y}\right)^2 S_I \\
S_{IV}' &= S_{IV} \\
S_V' &= S_V + \left(\frac{\delta\bar{y}}{y}\right)(S_{IV} + 3\, S_{III}) + 3\left(\frac{\delta\bar{y}}{y}\right)^2 S_{II} + \left(\frac{\delta\bar{y}}{y}\right)^3 S_I \\
S_{VI}' &= S_{VI} + \left(4\, S_V - 2\left(\frac{\bar{A}}{A}\right) S_{IV}\right)\left(\frac{\delta\bar{y}}{y}\right) \\
&\quad + (6\, S_{III} + S_{IV})\left(\frac{\delta\bar{y}}{y}\right)^2 + 4\, S_{II}\left(\frac{\delta\bar{y}}{y}\right)^3 + S_I\left(\frac{\delta\bar{y}}{y}\right)
\end{aligned}
$$

The conjugate shift functional dependence of the primary image aberrations (Shack, 1979) are more obscure. The formulae are derived by using the pupil aberration changes for a conjugate shift, because they are given by simple expressions, as opposed to the image aberrations which are much more complex. This fact can be seen by looking at the Seidel aberration equations.

$$S_I = A^2\, y\, \Delta\left(\frac{u}{n}\right)$$

$$S_{II} = A\,\bar{A}\, y\, \Delta\left(\frac{u}{n}\right)$$

$$S_{III} = \bar{A}^2\, y\, \Delta\left(\frac{u}{n}\right)$$

$$S_{IV} = -\mathcal{H}^2\, P$$

$$S_V = \left(\frac{\bar{A}}{A}\right)^3 S_I + \left(\frac{\bar{A}}{A}\right) S_{IV}$$

$$S_{VI} = \left(\frac{\bar{A}}{A}\right)^4 S_I + 2\left(\frac{\bar{A}}{A}\right) S_{IV}$$

For a stop shift only $\bar{A}$ changes while for a conjugate shift A, y and u all change. The equivalent pupil aberration equations are found simply by interchanging the chief and marginal ray definitions in the above set of equations which give the following

$$\bar{S}_I = \bar{A}^2\, \bar{y}\, \Delta\left(\frac{\bar{u}}{n}\right)$$

$$\bar{S}_{II} = \bar{A}\, A\, \bar{y}\, \Delta\left(\frac{\bar{u}}{n}\right)$$

$$\bar{S}_{III} = A^2\, \bar{y}\, \Delta\left(\frac{\bar{u}}{n}\right)$$

$$\bar{S}_{IV} = -\mathcal{H}^2\, P$$

$$\bar{S}_V = \left(\frac{A}{\bar{A}}\right)^3 \bar{S}_I + \left(\frac{A}{\bar{A}}\right) \bar{S}_{IV}$$

$$\bar{S}_{VI} = \left(\frac{A}{\bar{A}}\right)^4 \bar{S}_I + 2\left(\frac{A}{\bar{A}}\right)^2 \bar{S}_{IV}$$

A stop shift in this domain is equivalent to a conjugate shift in the image domain. Connecting the two sets the following set of equations are found.

$$S_I = \bar{S}_{VI} - \left(\frac{A}{\bar{A}}\right)\mathcal{H}\Delta(u^2) - \left(\frac{A}{\bar{A}}\right)^2 S_{IV} \qquad \bar{S}_I = S_{VI} + \left(\frac{\bar{A}}{A}\right)\mathcal{H}\Delta(\bar{u}^2) - \left(\frac{\bar{A}}{A}\right)^2 S_{IV}$$

$$S_{II} = \bar{S}_V - \mathcal{H}\Delta(u^2) \qquad \bar{S}_{II} = S_V + \mathcal{H}\Delta(\bar{u}^2)$$

$$S_{III} = \bar{S}_{III} - \mathcal{H}\Delta(u\bar{u}) \qquad \bar{S}_{III} = S_{III} + \mathcal{H}\Delta(u\bar{u})$$

$$S_{IV} = \bar{S}_{IV} \qquad \bar{S}_{IV} = S_{IV}$$

$$S_V = \bar{S}_{II} - \mathcal{H}\Delta(\bar{u}^2) \qquad \bar{S}_V = S_{II} + \mathcal{H}\Delta(u^2)$$

$$S_{VI} = \bar{S}_I - \left(\frac{\bar{A}}{A}\right)\mathcal{H}\Delta(\bar{u}^2) + \left(\frac{\bar{A}}{A}\right)^2 S_{IV} \qquad \bar{S}_{VI} = S_I + \left(\frac{A}{\bar{A}}\right)\mathcal{H}\Delta(u^2) + \left(\frac{A}{\bar{A}}\right)^2 S_{IV}$$

An object shift with respect to the pupil aberrations is simply given by the following

$$\bar{S}^*_I = \bar{S}_I$$

$$\bar{S}^*_{II} = \bar{S}_{II} + \bar{S}_I\left(\frac{\delta y}{\bar{y}}\right)$$

$$\bar{S}^*_{III} = \bar{S}_{III} + 2\,\bar{S}_{II}\left(\frac{\delta y}{\bar{y}}\right) + \bar{S}_I\left(\frac{\delta y}{\bar{y}}\right)^2$$

$$\bar{S}^*_{IV} = \bar{S}_{IV}$$

$$\bar{S}^*_V = \bar{S}_V + (\bar{S}_{IV} + 3\,\bar{S}_{III})\left(\frac{\delta y}{\bar{y}}\right) + 3\,\bar{S}_{II}\left(\frac{\delta y}{\bar{y}}\right)^2 + \bar{S}_I\left(\frac{\delta y}{\bar{y}}\right)^3$$

$$\bar{S}^*_{VI} = \bar{S}_{VI} + (4\,\bar{S}_{IV} - 2\left(\frac{A}{\bar{A}}\right)\bar{S}_{IV}\left(\frac{\delta y}{\bar{y}}\right) + (6\,\bar{S}_{III} + \bar{S}_{IV})\left(\frac{\delta y}{\bar{y}}\right)^2 + 4\,\bar{S}_{II}\left(\frac{\delta y}{\bar{y}}\right)^3 + \bar{S}_I\left(\frac{\delta y}{\bar{y}}\right)^4$$

Taking these formulae and substituting them into the connecting relationships between the image and pupil aberrations and using the following equations

$$\Delta^*(\bar{u}^2) = \Delta(\bar{u}^2)$$

$$\Delta^*(u\bar{u}) = \Delta(u\bar{u}) + \Delta(\bar{u}^2)\left(\frac{\delta y}{\bar{y}}\right)$$

$$\Delta^*(u^2) = (u^2) + 2\Delta(u\bar{u})\left(\frac{\delta y}{\bar{y}}\right) + (\bar{u}^2)\left(\frac{\delta y}{\bar{y}}\right)^2$$

$$\left(\frac{A}{\bar{A}}\right)^* = \left(\frac{A}{\bar{A}}\right) + \left(\frac{\delta y}{\bar{y}}\right)$$

the conjugate shift equations are arrived at:

$$S_I^* = S_I + (3S_{II}+\bar{S}_V)\frac{\delta y}{\bar{y}} + (3S_{III}+3\bar{S}_{III}+2S_{IV})\left(\frac{\delta y}{\bar{y}}\right)^2 + (3\bar{S}_{II}+S_V)\left(\frac{\delta y}{\bar{y}}\right)^3 + \bar{S}_I\left(\frac{\delta y}{\bar{y}}\right)^4$$

$$S_{II}^* = S_{II} + (2S_{III}+S_{IV}+\bar{S}_{III})\left(\frac{\delta y}{\bar{y}}\right) + (S_V+2\bar{S}_{II})\left(\frac{\delta y}{\bar{y}}\right)^2 + \bar{S}_I\left(\frac{\delta y}{\bar{y}}\right)^3$$

$$S_{III}^* = S_{III} + (S_V+\bar{S}_{II})\left(\frac{\delta y}{\bar{y}}\right) + \bar{S}_I\left(\frac{\delta y}{\bar{y}}\right)^2$$

$$S_{IV}^* = S_{IV}$$

$$S_V^* = S_V + \bar{S}_I\left(\frac{\delta y}{\bar{y}}\right)$$

Structural Aberration Approach To Pupil Aberrations

Following Shack's development for the structural aberration coefficients of the image a corresponding development can be given for the pupil aberrations. Using the connecting relationships between the two sets of aberrations the following coefficeints give a consistent set of equations for image space.

$$\bar{S}_I = \frac{4\mathcal{H}^4 \bar{\sigma}_I}{y_P^4 \phi}$$

$$\bar{S}_{II} = \frac{2\mathcal{H}^3 \bar{\sigma}_{II}}{y_P^2}$$

$$\bar{S}_{III} = \mathcal{H}^2 \phi \bar{\sigma}_{III}$$

$$\bar{S}_{IV} = \mathcal{H}^2 \phi \bar{\sigma}_{IV}$$

$$\bar{S}_V = \frac{1}{2} \mathcal{H} y_p^2 \phi^2 \bar{\sigma}_V$$

$$\bar{S}_{VI} = \frac{1}{4} y_P^4 \phi^3 \bar{\sigma}_{VI}$$

Using the structural aberration coefficients in the conjugate shift equations give the following

$$\sigma_I^* = \sigma_I + (3\sigma_{II}+\bar{\sigma}_V)\bar{S} + (3\sigma_{III}+2\sigma_{IV}+3\bar{\sigma}_{III})\bar{S}^2 + (\sigma_V+3\bar{\sigma}_{II})\bar{S}^3 + \bar{\sigma}_I \bar{S}^4$$

$$\sigma_{II}^* = \sigma_{II} + (2\sigma_{III}+\sigma_{IV}+\bar{\sigma}_{III})\bar{S} + (\sigma_V+2\bar{\sigma}_{II})\bar{S}^2 + \bar{\sigma}_I \bar{S}^3$$

$$\sigma_{III}^* = \sigma_{III} + (\sigma_V+\bar{\sigma}_{II})\bar{S} + \bar{\sigma}_I \bar{S}^2$$

$$\sigma_{IV}^* = \sigma_{IV}$$

$$\sigma_V = \sigma_V + \bar{\sigma}_I \bar{S}$$

$\bar{S}$ is the object shift factor which is determined by the initial system from which one is shifting the object. For the initial system pictured below

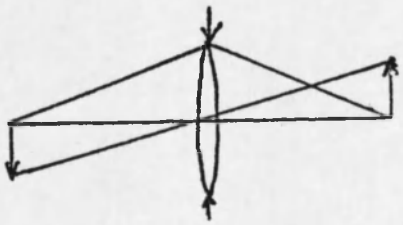

Y = 0

the structural aberration conjugate shift formula become

$$\sigma_I^* = \sigma_I - (3\sigma_{II}+\bar{\sigma}_V)Y + (3\sigma_{III}+2\sigma_{IV}+3\bar{\sigma}_{III})Y^2 - (\sigma_V+3\bar{\sigma}_{II})Y^3 + \bar{\sigma}_I Y^4$$

$$\sigma_{II}^* = \sigma_{II} - (2\sigma_{III}+\sigma_{IV}+\bar{\sigma}_{III})Y + (\sigma_V+2\bar{\sigma}_{II})Y^2 - \bar{\sigma}_I Y^3$$

$$\sigma_{III}^* = \sigma_{III} - (\sigma_V+\bar{\sigma}_{II})Y + \bar{\sigma}_I Y^2$$

$$\sigma_{IV}^* = \sigma_{IV}$$

$$\sigma_V^* = \sigma_V - \bar{\sigma}_I Y$$

APPENDIX B

THE Y-$\bar{Y}$ DIAGRAM

Basic terms

y - marginal ray height

$\bar{y}$ - chief ray height

u - angle between axis and marginal ray

$\bar{u}$ - angle between axis and chief ray

$\mathcal{H}$ - Lagrange invariant

Reduced terms

$\tau = t/n$

$\omega = nu$

$\bar{\omega} = n\bar{u}$

Basic equations

Lagrange invariant: $$\mathcal{H} = \bar{\omega}y - \omega\bar{y}$$

axial distance: $$\tau = \frac{\begin{vmatrix} y_1 & \bar{y}_1 \\ y_2 & \bar{y}_2 \end{vmatrix}}{\mathcal{H}}$$

power: $$\phi = \frac{\begin{vmatrix} \omega_1 & \bar{\omega}_1 \\ \omega_K^1 & \bar{\omega}_K^1 \end{vmatrix}}{\mathcal{H}}$$

LIST OF REFERENCES

ACCOSV, Scientific Calculations, Inc., Rochester, NY (1971).

Blandford, B.A.F., Optical Instruments and Techniques, Oriel, Newcastle-Upon-Tyne, 435-443 (1970).

Delano, E., "First-order design and the Y-$\bar{Y}$ diagram," Appl. Opt. 2, 1251 (1963).

Duffieux, P. M., L'Integrale de Fourier et ses Applications a L'Optique, Faculte des Sciences, Besancon (1946).

Gaskill, J. G., Linear Systems, Fourier Transforms, and Optics, Wiley and Sons, NY (1978).

Goodman, J. W., Introduction to Fourier Optics, McGraw-Hill, NY (1968).

Harris, T. I., "Fourier transform lens problem," International Lens Design Conference, Haverford (1975).

Hopkins, G., "Aberrational analysis of optical systems: A proximate ray tracing approach," Ph. D. dissertation, Optical Sciences Center, University of Arizona, Tucson (1976).

Hopkins, H., "Image formation with coherent and partially coherent light," JSPSE. 2, 114 (1977).

Offner, A., "New concepts in projection mask aligners," Opt. Eng. 14, 131 (1975).

O'Neill, E. L., "Spatial filtering in optics," IRE Trans. Inform. Theory IT-2, 56 (1956).

Shack, R. V., "Analytic system design with pencil and ruler--the advantages of the Y-$\bar{Y}$ diagram," SPIE Proceedings 39, 127 (1973).

Shack, R. V., "The use of normalization in the application of simple optical systems," SPIE Proceedings 54, 155 (1974).

Shack, R. V., Professor, Optical Sciences Center, University of Arizona, Tucson, private communication (1979).

Vander Lugt, A., "Operational notation for the analysis and synthesis of optical data-processing systems," Proc. of IEEE 54, 1055 (1966).

Vatz, B., Specification and error budgeting of optical signal processors BMDATC-R, U. S. Army Ballistic Missile Defense Advanced Technology Center (1977).

Welford, W. T., Aberrations of the Symmetrical Optical System, Academic Press, London (1974).

Wynne, C. G., "Primary aberrations and conjugate change," Proc. Phys. Soc. London B65, 429 (1952).

Wynne, C. G., "Simple Fourier transform lenses--I and II, Optical Comm. 12, 266 and 270 (1974).